UNIVERSITÀ DEGLI STUDI DELL'INSUBRIA

Facoltà di Scienze Matematiche, Fisiche e Naturali

Dottorato di Ricerca in Astronomia e Astrofisica

Tesi di Dottorato

THE OBSERVABILITY OF ISOLATED NEUTRON STARS AND BLACK HOLES

Supervisor:

Prof. Aldo Treves

Nicola Sartore

Matricola 708043

XXIII^o Ciclo

Contents

PREFACE **5**

1 INTRODUCTION **7**

1.1 Neutron stars 7

1.2 Black holes 10

1.3 The past 40 years 10

2 MONTE CARLO SIMULATIONS OF NEUTRON STAR ORBITS **19**

2.1 Method 20

2.1.1 Distribution of progenitors 20

2.1.2 Birth velocities 26

2.1.3 Gravitational potential 28

2.1.4 Orbit Integration 32

2.2 Results of the simulation 36

2.2.1 Fraction of bound neutron stars 36

2.2.2 Distribution of heights 38

2.2.3 Neutron stars in the disk 40

2.2.4 Mean velocities 40

2.2.5 The solar neighbourhood 43

2.2.6 Neutron stars in the halo 44

2.2.7 Sky density of neutron stars 44

2.2.8 Results with different potential 48

2.3 Summary of the results 48

3 MICROLENSING FROM ISOLATED NEUTRON STARS AND BLACK HOLES **51**

3.1 The microlensing phenomenon 51
3.2 Basic theory of microlensing 53
3.3 Model of the Galaxy 56
3.3.1 Distribution of normal stars 56
3.3.2 Updated distribution of neutron stars and black holes . 57
3.4 Results 61
3.4.1 Optical depth 61
3.4.2 Rate of events and distribution of time-scales 62
3.4.3 Comparison with previous simulations 70
3.5 Discussion of the results 74

4 COUNTERPARTS OF CANDIDATE BLACK HOLE LENSES 77

4.1 Method 78
4.1.1 Catalogues of microlensing events 78
4.1.2 Catalogues of X-ray sources 79
4.1.3 Cross-correlation analysis 79
4.2 Results of the cross-correlation 82
4.3 The nature of 2XMM J180540.5-273427 87

5 SUMMARY AND CONCLUSIONS 89

A Coefficients of the fits 93

List of publications 97

Bibliography 101

PREFACE

The detection of old neutron stars and black holes in isolation is one of the cornerstones of compact object astrophysics. However, forty years after the first pioneering studies, no succesful candidates have been found to confirm the early predictions, making the search for old isolated compact objects a still open and intriguing subject. The scope of this thesis is thus to investigate the observability of isolated neutron stars and black holes with the final objective of defining new possible strategies for the long-sought detection of these elusive objects.

The thesis is organized as follows. In Chapter 1, after a short discussion on the origin of neutron stars and stellar-mass black holes in isolation, I summarize the results of past efforts made to constrain their observational properties.

In Chapter 2 I tackle with the dynamics of isolated neutron stars. I describe the set-up of a numerical Monte Carlo code, named Population SYnthesis of Compact Objects (PSYCO in brief), developed as part of the PhD project. I then present the results of the simulation, with particular emphasis for statistical properties of neutron stars in the Galactic disk and in the solar neighbourhood. These first results will be used as base to explore alternative methods to detect old neutron stars and black holes. It should be noted that, following the standard practice, these first results are obtained considering only neutron stars born in the disk of the Milky Way. As it will be shown in Chapter 3, the contribution of neutron stars, and black holes, born in the Galactic bulge cannot be neglected since they could represent the majority of detectable objects.

In Chapter 3 the feasibility of microlensing as a technique to detect isolated neutron stars and black holes is explored, making use of the results

illustrated in the previous Chapter. After an overview of results obtained so far by the several surveys, I describe the basic microlensing quantities and expressions. I then describe the models adopted in my work for the distribution of bulge and disk stars, to which the contribution of neutron stars and black holes is then compared to. I compare the optical depth and event rate due to neutron stars and black holes with that of normal stars. Also, I study the distribution of event time-scales in both cases.

After the results reported in Chapter 3, in Chapter 4 I present a systematic cross-correlation analysis of microlensing events with the catalogues of X-ray sources of the XMM-Newton and Chandra satellites, which appeared recently. I report the results of the cross-correlation and the properties of a source resulting from the cross-correlation procedure.

Finally, in Chapter 5 I review the results of my PhD project and draw the final conclusion. I also discuss possible future developments.

1 INTRODUCTION

Neutron stars and stellar-mass black holes are born mainly in the core-collapse of a massive star, with mass greater than $\sim 8\,M_{\odot}$ (where $1\,M_{\odot}$ is equal to a solar mass), which exhausted its thermonuclear fuel. Hence, the star is not able any more to sustain its own gravity and the core-collapse occurs. The final outcome of this process depends on the physical properties of the progenitor like, for example, its mass and chemical composition (e.g. Heger et al., 2003).

Neutron stars and black holes can be formed also through accretion-induced collapse of stars in binary systems, (e.g. Lorimer, 2008, and references therein). However, the outcome of the collapse is strongly affected by the complex interactions between the two stars in the binary rather than being dependent only on the initial properties of the collapsing stars. Furthermore, the frequency of accretion-induced collapses is much lower than the case of isolated massive stars (Arnett et al., 1989). Thus, isolated neutron stars and black holes should represent the bulk of the population in the Milky Way.

1.1 Neutron stars

The formation of a neutron star happens when the pressure of degenerate neutrons formed by inverse β decay in the collapsing core is able to balance the gravitational force. The external envelope of the the progenitor star is then ejected at high speed, $\sim 10^4\,\mathrm{km\,s^{-1}}$, in a powerful supernova explosion. Such events can be observed even at cosmological distances.

After birth, the observational appearance of neutron stars varies a lot among single objects and it too depends on their intrinsic properties, like

magnetic field strength and angular momentum. The large majority of known neutron stars has been detected as young isolated pulsars, powered by magneto-rotational losses and detected through radio or gamma-ray observations.

The advent of X-ray astronomy allowed the discovery of other classes of isolated neutron stars that are not shining at radio or gamma-ray wavelengths. In these objects the emission comes from the dissipation of the magnetic field and/or residual heat as in magnetars or in XDINS and CCOs (X-ray Dim Isolated Neutron Stars and Central Compact Objects respectively, see e.g. Mereghetti 2008; Turolla 2009 for reviews).

Anyway, whatever the nature of their energy reservoir is, the emission of isolated neutron stars is expected to fade away in a time-scale much shorter than the age of the Milky Way, which is $\sim 10^{10}$ years. Considering that the typical lifetime of a massive star is $\lesssim 10^7$ years and that our Galaxy likely produced such massive stars throughout its existence, a large number of "exhausted" neutron stars is thus expected to be harboured in it.

From estimates of nucleosynthesis yields by core-collapse supernovae, Arnett et al. argued that as many as $\sim 10^9$ of such events should have occurred in our Galaxy, the large majority leaving a neutron star as remnant (Fig. 1). However, a more recent estimate of the core-collapse rate was obtained by Diehl et al. (2006) from measurements of the gamma-ray emission of ^{26}Al in the interstellar medium, and returned a value of ~ 2 per century. This implies that, assuming a constant star formation rate throughout the existence of the Galaxy, $\sim 2 \times 10^8$ neutron stars have been born in it.

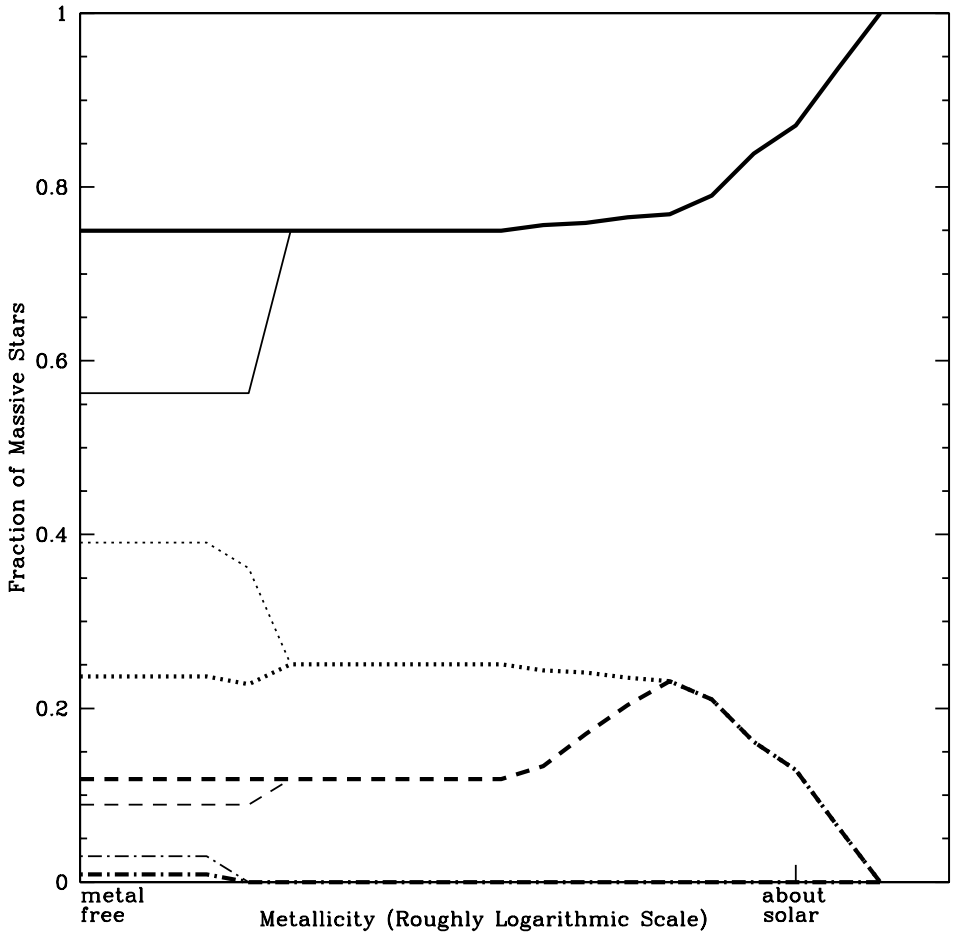

Figure 1: Fraction of massive stars that form neutron stars (solid lines) and black holes (dotted lines). Different line styles represent different initial mass functions. Source: Heger et al. (2003).

1.2 Black holes

Stellar-mass black holes are the final evolutionary phase of very massive stars. Stars with initial mass $M \gtrsim 40\,M_{\odot}$ are expected to undergo direct collapse into a black hole, without generating a supernova. However, black holes could form also by accretion of fall-back material onto a new-born neutron star, if the mass of the progenitor is in the range $25\,M_{\odot} \lesssim M \lesssim 40\,M_{\odot}$ (Heger et al., 2003). Furthermore, the composition of the progenitor plays an important role: for metallicities above the solar one, the amount of mass lost through stellar wind can be so large that even the most massive stars end their lives as neutron stars rather than leaving a black hole as remnant (Figure 2). This scenario has possibly been confirmed by the detection of a magnetar, CXO J164710.2-455216, associated with the massive star cluster Westerlund 1. The turn-off point of the cluster is around $\sim 35\,M_{\odot}$, implying that the initial mass of the progenitor of CXO J164710.2-455216 should have been $\gtrsim 40\,M_{\odot}$ (Muno et al., 2006).

Nevertheless, a crude estimate of the number of Galactic black holes can be obtained from the stellar initial mass function (e.g. Salpeter, 1955; Kroupa, 2001): the ratio between the number of black holes and neutron stars is $\sim 0.1 - 0.2$. This yields a number of Galactic black holes between several times 10^7 and $\sim 10^8$.

1.3 The past 40 years

The detection of this large population of old neutron stars and stellar-mass black holes in isolation would be of paramount importance. Their distribution in phase-space could, for example, act as a probe of the gravitational potential of the Milky Way, as well as to give precious insights on the magni-

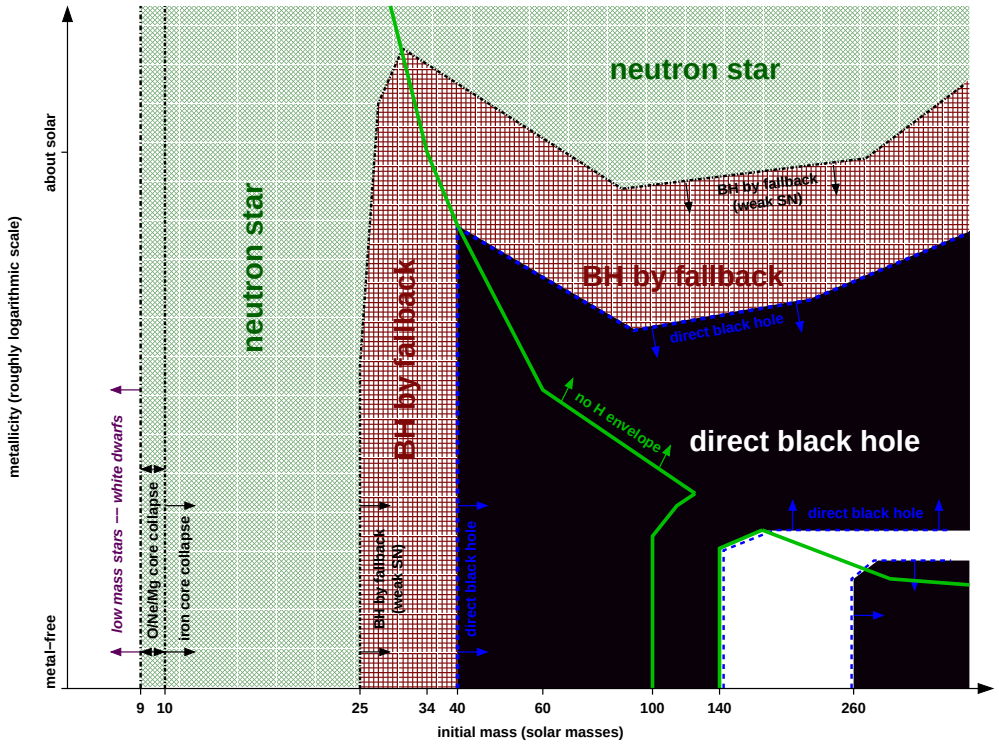

Figure 2: Remnants of single massive stars as a function of the initial metallicity (y-axis) and initial mass (x-axis). Source: Heger et al. (2003)

tude of natal kicks received by neutron stars and possibly also by black holes at birth. This fact may itself help to constrain the physical mechanism responsible for these kicks. Useful information about the star formation history of the Milky Way could be also retrieved.

The search for old neutron stars and black holes in isolation has been tackled by many authors in the past. Ostriker et al. (1970) proposed that old neutron stars could be recycled by accretion from the interstellar medium, under the hypothesis of spherical accretion (Bondi & Hoyle, 1944; Bondi, 1952). Assuming a velocity with respect to the medium $v \sim 10\,\mathrm{km\,s^{-1}}$, a density of the medium $n \sim 1\,\mathrm{cm^{-3}}$ and the canonical values of $M = 1.4\,M_\odot$ and $R = 10^6\,\mathrm{cm}$ respectively for the mass and radius of a neutron star, they found that the accretion luminosity would be

$$L = \frac{G\,M\,\dot{M}}{R} \sim 2 \times 10^{31} \Big(\frac{\dot{M}}{10^{11}\,\mathrm{g\,s^{-1}}} \Big)\,\mathrm{erg\,s^{-1}}\,, \tag{1.1}$$

where

$$\dot{M} = \frac{2\pi (GM)^2 m_p n}{(v^2 + c_s^2)^{3/2}} \sim 10^{11} n v_{10}^{-3}\,\mathrm{g\,s^{-1}}\,, \tag{1.2}$$

is the accretion rate according to the Bondi-Hoyle-Littleton theory, m_p is the mass of the proton, c_s is the sound of speed of the medium and $v_{10} = (v^2 + c_s^2)^{3/2}/(10\,\mathrm{km\,s^{-1}})$. The temperature kT, assuming blackbody emission, would be $\sim 100\,\mathrm{eV}$, that is in the soft X-rays.

The launch of the ROSAT satellite, with its good sensitivity in the soft X-ray band, gave boost to the search of isolated neutron stars and black holes, especially the former since, being more numerous than black holes,

they were expected to represent the bulk of likely detections. Adopting the results of numerical simulation of Paczynski (1990), Treves & Colpi (1991) predicted the hundreds to thousands accreting old neutron stars would be potentially observable by ROSAT. Similar predictions were made by Blaes & Madau (1993). However, only a handful of isolated neutron stars have been discovered by ROSAT (e.g. Walter & Matthews 1997). These are commonly accepted as middle-aged cooling neutron star, the aforementioned XDINS, likely born in close-by star-forming regions (Popov et al., 2005; Posselt et al., 2008).

Theoretical models of accretion from the interstellar medium have been developed in a similar fashion also for black holes (see e.g. Campana & Pardi, 1993; Agol & Kamionkowski, 2002; Beskin & Karpov, 2005; Mapelli et al., 2006). However, predictions for black holes are afflicted by larger uncertainties since the only useful information about their statistical properties derives from few known objects in X-ray binaries. On the other hand, the phase-space distribution of isolated black holes is completely unconstrained.

The lack of isolated accreting neutron stars and black holes (e.g. Neuhäuser & Trümper 1999) has more than one possible explanation. First, the spherical accretion rate is strongly dependent of the relative velocity between the accreting object and the surrounding medium (cfr. Equation 1.2). Popov et al. (2000) explored the observability of accreting old neutron stars for a wide range of initial mean velocities, between 0 and 550 $\mathrm{km\,s^{-1}}$, assuming a Maxwellian distribution. The observed paucity of accretors in the ROSAT catalogue would be explained if neutron stars are born with average velocities of at least $200\,\mathrm{km\,s^{-1}}$, that is a factor ~ 10 larger than the dispersion velocity of normal stars in the Galactic disk. Therefore the accretion rate would be a factor $\sim 10^3 - 10^4$ lower than that predicted by Treves & Colpi. The large

spatial velocities of neutron stars have been confirmed by measurements of the proper motions of known young neutron stars (see Chapter 2).

Second, neutron stars are born with very strong magnetic fields, $B \sim 10^{11} - 10^{15}\,\mathrm{G}$, and with short spin periods, $P \sim 30 - 100\,\mathrm{ms}$. These facts put stringent constraints on the conditions for which the accretion flow can penetrate the magnetosphere of the neutron star (see e.g. Treves et al., 2000). The first condition is that the Alfvén radius, that is the radius inside which the dynamics of the infalling matter is dominated by the magnetic field (Illarionov & Sunyaev, 1975)

$$\begin{aligned} r_A &= \Big(\frac{B^2\,R^6}{\sqrt{2GM}\dot{M}}\Big)^{2/7} \qquad (1.3)\\ &\sim 2\times 10^{10}\Big(\frac{B}{10^{12}\,\mathrm{G}}\Big)^{4/7}\Big(\frac{\dot{M}}{10^{11}\,\mathrm{g\,s^{-1}}}\Big)^{-2/7}\Big(\frac{R}{10^{6}\,\mathrm{cm}}\Big)^{12/7}\Big(\frac{M}{M_\odot}\Big)^{-1/7}\,\mathrm{cm}\,, \end{aligned}$$

must be smaller of the accretion radius

$$r_{accr} = \frac{2GM}{v^2} \sim 3\times 10^{14}\Big(\frac{M}{M_\odot}\Big)v_{10}^{-2}\,\mathrm{cm}\,, \qquad (1.4)$$

which defines the region where the dynamics of the interstellar medium is dominated by the gravitational field of the neutron star. The second condition is that the gravitational energy density of the infalling matter at accretion radius

$$U_G = \frac{GMm_p n}{r} \sim 6.5\times 10^{-13}\Big(\frac{\dot{M}}{10^{11}\,\mathrm{g\,s^{-1}}}\Big)\Big(\frac{r}{10^{14}\,\mathrm{cm}}\Big)^{-5/2}\,\mathrm{erg\,cm^{-3}}\,, \qquad (1.5)$$

must be greater than the energy density of the outflowing electromagnetic dipole radiation

$$\begin{aligned} U_B &= \Big(\frac{B^2}{8\pi}\Big)\Big(\frac{R^6}{r_c^6}\Big)\Big(\frac{r_c^2}{r^2}\Big) \\ &\sim 7.5\times 10^{-19}\Big(\frac{B}{10^{12}\,\mathrm{G}}\Big)^2 P^{-4}\Big(\frac{r}{10^{14}\,\mathrm{cm}}\Big)^{-2}\,\mathrm{erg cm^{-3}}\,, \end{aligned} \tag{1.6}$$

where $r_c = cP/2\pi$ is the light cylinder radius. This translates into a condition on the spin period, which must be larger than a critical value

$$\begin{aligned} P &\gtrsim P_{crit} \\ &\sim 10\Big(\frac{B}{10^{12}\,\mathrm{G}}\Big)^{1/2}\Big(\frac{\dot{M}}{10^{11}\,\mathrm{g\,s^{-1}}}\Big)^{-1/4}\Big(\frac{r_A}{10^{14}\,\mathrm{cm}}\Big)\Big(\frac{R}{10^{6}\,\mathrm{cm}}\Big)^{3/2}\Big(\frac{M}{M_\odot}\Big)^{1/8}\mathrm{s}\,. \end{aligned} \tag{1.7}$$

As Blaes & Madau have pointed out, the time-scale necessary for an isolated neutron star to slow down its rotation to $P \gtrsim P_{crit}$ is of the same order of the age of the Galaxy. This would mean that in many cases the conditions for accretion could be hardly reached during the neutron star life. Furthermore, even if $P > P_{crit}$, the gravitational acceleration of the infalling matter at the Alfvén radius should be larger than the centrifugal acceleration due to the rotating magnetosphere

$$\Big(\frac{GM}{r_A^2}\Big) \gtrsim \Big(\frac{2\pi}{P}\Big)^2 r_A\,. \tag{1.8}$$

This fact puts another stronger constraint on the spin period

$$P \gtrsim P_A \sim 10^3 \Big(\frac{B}{10^{12}\,\mathrm{G}}\Big)^{6/7} \Big(\frac{\dot{M}}{10^{11}\,\mathrm{g\,s^{-1}}}\Big)^{-1/2} \Big(\frac{M}{M_\odot}\Big)^{-1/2} \mathrm{s}\,.$$

As discussed by Treves et al., a neutron stars in this phase should give away much of its angular momentum to allow accretion. The torque exerted by matter accumulated at the Alfvén radius could enhance the rate at which the angular momentum is lost with respect to magneto-dipole losses alone, thus shortening the time needed to reach the accretion phase. However, Colpi et al. (1998) showed that, if the magnetic fields decays with a time scale $\lesssim 10^9$ years, the rate at which the neutron star looses its angular momentum decreases and thus the accretion phase may not be reached. In any case, the decay of the magnetic field in neutron stars has not been observed to date (e.g. Lorimer et al., 1997) and its occurrence is still matter for debate.

Recent two-dimensional magnetohydrodynamical (MHD) simulations of low-rate accretion onto a magnetized neutron star (Toropina et al., 2003) suggest that the presence of a weak magnetic field in the accreted medium could also lead to the suppression of the accretion rate. The plasma would be compressed adiabatically during the infall, thus increasing the strength of its magnetic field. When equipartition is reached the magnetic field would start to reconnect, thus heating the gas and modifying its properties. The suppression factor would be $\sim (r_A/r_{accr})^p$ with p being of the order of unity (Perna et al., 2003, and references therein).

Another factor that could influence the statistics of accreting neutron stars and black holes arises from fact that the spatial distribution of the interstellar medium is patchy rather than smooth. This implies that the probability of a neutron star or a black hole residing in a medium-rich region is small (e.g. Agol & Kamionkowski, 2002). All the mentioned factors

act together to hinder the accretion from the interstellar medium and can successfully explain the paucity of detections of accreting isolated remnant.

In addition to the suppressing effect on the accretion rate, the large velocities observed in neutron stars, and possibily also in black holes, can have a deep impact on their present phase-space distribution. Hence, a first step to define new methods to detect isolated remnants is to determine where these objects stand with respect to an observer at the Earth's position. To this purpouse, a simulation of neutron star orbits in the Galactic potential is presented in the next Chapter.

2 MONTE CARLO SIMULATIONS OF NEUTRON STAR ORBITS

The number of known young neutron stars is $\sim 2 \times 10^3$ and it is growing steadily. Thus, the knowledge on their statistical properties is being constantly refined and it can be used as starting point to model the properties of the of old neutron star , whose distribution in phase-space can therefore be reconstructed with a certain degree of confidence with population synthesis models.

There is mounting evidence that isolated neutron stars are born with very large spatial velocities. For example, radio pulsars show spatial velocities of several hundreds $\mathrm{km\,s^{-1}}$ (e.g. Arzoumanian et al., 2002; Hobbs et al., 2005; Faucher-Giguère & Kaspi, 2006). Some radio pulsars exhibit velocities in excess of 1000 $\mathrm{km\,s^{-1}}$. A striking example is the radio pulsar PSR B1508+55: the proper motion and parallax measurements obtained from radio observations point to a transverse velocity of $\sim 1083\,\mathrm{km\,s^{-1}}$ (Chatterjee et al., 2005).

Similar high values of the velocity have also been inferred for objects belonging to other classes of young isolated neutron stars . Thanks to Chandra observations, Hui & Becker (2006) estimated a velocity of $\sim 1100\,\mathrm{km\,s^{-1}}$ for the Central Compact Object RX J0822-4300. Recently Motch et al. (2009) measured the proper motion of three XDINSs (RX J0420.0-5022, RX J0806.4-4123 and RX J1308.6+2127) and inferred velocities of $600 - 1000\,\mathrm{km\,s^{-1}}$. This is not uncommon in young isolated neutron stars and hence they concluded that the velocity distribution of the XDINS is not statistically different from that of normal radio pulsars.

The origin of such high velocities is not clear. An asymmetric supernova

explosion is considered one possible explanation (Dewey & Cordes, 1987). Iben & Tutukov (1996) argued that the effects of binary disruption may also contribute to the observed velocities. Recently it has been proposed that the fastest neutron stars are the remnants of runaway progenitors expelled via N-body interactions from the dense core of young star clusters (Gvaramadze et al., 2008).

These large velocities, no matter how they are achieved, are of the same order of magnitude of the escape velocity from the Milky Way and therefore have a strong impact on the phase-space distribution of old neutron stars. A large fraction of them could have escaped from the Milky Way during its life-time, thus lowering the density of neutron stars in the Galaxy and, as a consequence, the probability to detect these object.

2.1 Method

In the following, I describe the set-up of the numerical code used to characterize the distribution in phase-space of old neutron stars. I adopt the same approach of Paczynski (1990). Initial conditions (position, velocity) are assigned randomly from the selected distributions to each simulated neutron star by means of a Monte Carlo procedure.

2.1.1 Distribution of progenitors

The initial positions of neutron stars in the Galaxy are defined in a galactocentric cylindrical coordinates system (R, ϕ, z), where the z axis corresponds to the axis of rotation of the Milky Way. These initial positions reflect the distribution of their progenitors: according to Bronfman et al. (2000), formation of massive stars is currently concentrated in an annular region which follows the distribution of molecular hydrogen. However, to explore the effects of

the distributions of progenitors on the current phase-space configuration of neutron stars, I choose four possible distribution models from the literature.

Paczynski suggested an exponential probability distribution, based of the observed surface brightness[1] of face-on Sc galaxies

$$p(R)\,dR = a_R \frac{R}{R_{exp}^2} \exp\Big(-\frac{R}{R_{exp}}\Big)\,dR\,, \tag{2.1}$$

where $p(R)dR$ is the probability that a neutron star is born between R and $R + dR$, $R_{exp} = 4.5\,\mathrm{kpc}$ is the scale-length of the Galactic disk and $a_R = 1.0683$ is a normalization factor.

Bronfman et al. obtained the aforementioned radial distribution of star-forming regions in the Milky Way from the combined far infrared and millimetric emission produced by clusters of massive stars embedded in ultra-compact HII regions. The far infrared (surface) luminosity, $\rho(R)$, has a Gaussian shaped rise until it reaches a maximum at $\sim 4.7\,\mathrm{kpc}$. (full width at half maximum of 2.38 kpc), then it decays exponentially, with a scale-length of 1.78 kpc, towards the outer part of the Galaxy, following the distribution of neutral hydrogen. The radial birth probability is thus obtained from the far infrared luminosity from the equation

$$p(R)\,dR = \frac{R\,\rho(R)\,dR}{\int_0^\infty R\,\rho(R)\,dR}\,. \tag{2.2}$$

Another possible distribution of neutron star progenitors can be obtained from the surface density of Galactic supernova remnants (Case & Bhattacharya, 1998)

[1] In the J band.

$$\rho(R) = \left(\frac{R}{R_0}\right)^{\alpha} \exp\left[-\frac{\beta(R-R_0)}{R_0}\right], \tag{2.3}$$

where $\alpha = 2$ and $\beta = 3.53$ and $R_0 = 8.5\,\mathrm{kpc}$. The corresponding radial probability density is again obtained from Equation 2.2.

The fourth radial distribution adopted has been proposed by Faucher-Giguère & Kaspi (2006)

$$p(R) = \frac{1}{\sqrt{2\pi}\sigma} \exp\left[-\frac{(R-R_{peak})^2}{2\sigma^2}\right], \tag{2.4}$$

where $R_{peak} = 7.04\,\mathrm{kpc}$ and $\sigma = 1.83\,\mathrm{kpc}$. This distribution has been extrapolated from the observed distribution of radio pulsars found by Yusifov & Küçük (2004). Hereafter these distribution models are labelled as models 1, 2, 3 and 4, respectively. Finally, for all models I assume that neutron stars can be generated from 0 to 20 kpc.

Massive stars are located in the spiral arms of the Milky Way, they are indeed the ideal tracers of the spiral structure. Thus spiral arms are considered in the distribution of neutron star progenitors, adopting the same prescription of Faucher-Giguère & Kaspi: massive stars are distributed along four logarithmic spirals, each spiral described by the equation

$$\phi(R) = k\,\ln(R/R_*) + \phi_0\,. \tag{2.5}$$

The values of the parameters k, R_* and ϕ_0 for each spiral are given in Table 1. Actually, Equation 2.5 describes the position of arm centroids. A

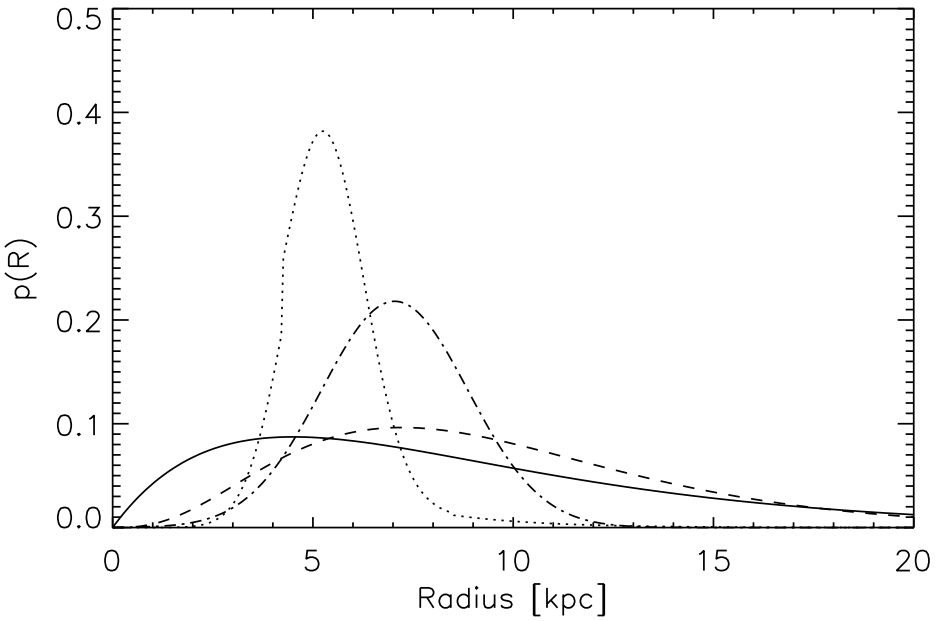

Figure 3: Radial probability distributions of neutron star progenitors. Line styles depict the models of Paczynski 1990, (solid, model 1), Bronfman et al. 2000, (dotted, model 2), Case & Bhattacharya 1998, dashed, model 3 and Faucher-Giguère & Kaspi 2006, (dot-dashed, model 4), respectively.

Table 1: Parameters of the spiral arms.

Arm	k	R_* [kpc]	ϕ_0 [radians]
Norma	4.25	3.48	1.57
Carina-Sagittarius	4.25	3.48	4.71
Perseus	4.89	4.90	4.09
Crux-Scutum	4.89	4.90	0.95

more realistic distribution can be obtained if the positions of progenitors are scattered, both in the radial and azimuthal directions, around these centroids, see Figure 4. Details on how the scatter is added to the initial positions of neutron stars can be found in the paper of Faucher-Giguère & Kaspi.

The thickness of the star-forming region is few tens of parsec (Bronfman et al., 2000; Maíz-Apellániz, 2001). However, as Sun & Han (2004) have pointed out, the long term dynamical behaviour of a population of neutron stars is insensitive to the scale-height of its progenitors (see also Kiel & Hurley 2009). Following these results I assume that all neutron stars are born on the Galactic plane, that is $z_i = 0$.

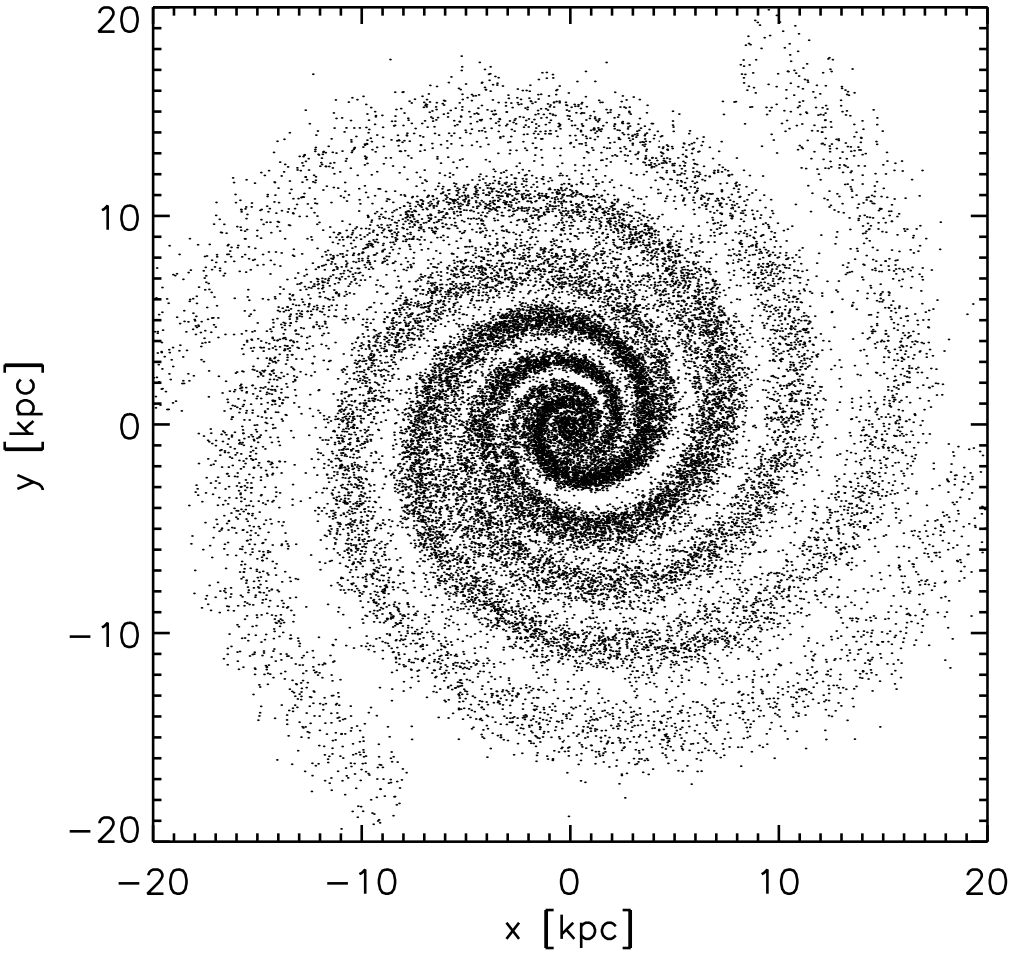

Figure 4: Projection on the (X, Y) plane of initial positions of neutron stars, where $X = R\cos\phi$ and $Y = R\sin\phi$. - The radial distribution is from Paczynski (1990). The position of the Sun is at $(X, Y) = (8.5, 0.0)$.

2.1.2 Birth velocities

The true form of the distribution of birth velocities is still a hotly debated issue. For example, Lorimer et al. (1997) and Hobbs et al. (2005) proposed a Maxwellian distribution

$$p(v) = \sqrt{\frac{2}{\pi}} \frac{v^2}{\sigma^3} \exp\Big(- \frac{v^2}{2\,\sigma^2} \Big) . \tag{2.6}$$

where v is the three-dimensional velocity and σ is the velocity dispersion. Alternatively, Arzoumanian et al. (2002) and Brisken et al. (2003) proposed a bimodal distribution

$$p(v) = \sqrt{\frac{2}{\pi}}\, v^2 \left[\frac{w}{\sigma_1^3} \exp\Big(- \frac{v^2}{2\,\sigma_1^2} \Big) + \frac{1-w}{\sigma_2^3} \exp\Big(- \frac{v^2}{2\,\sigma_2^2} \Big) \right] \tag{2.7}$$

where w is the relative weight of the two sub-distributions and σ_1 and σ_2 are the respective velocity dispersions.

Using the same sample of pulsars of Brisken et al., Faucher-Giguère & Kaspi explored, together with single and bimodal Maxwellian models, also other possible distribution functions like the double-sided exponential

$$p(v_i) = \frac{1}{2\,v_{exp}} \exp\Big(- \frac{|v_i|}{v_{exp}} \Big) , \tag{2.8}$$

where v_i represents a single component (v_R, v_ϕ or v_z) of the spatial velocity and v_{exp} is a characteristic velocity; the Lorentzian

$$p(v_i) = \frac{1}{\pi\,\gamma \left(1 + \left(v_i^2 / \gamma^2 \right) \right)} , \tag{2.9}$$

where γ is a scale parameter defining the half-width at half-maximum, and the distribution proposed by Paczynski

$$p(v) = \frac{4}{\pi\, v_* \left(1 + \left(v/v_*\right)^2\right)^2}\,, \tag{2.10}$$

where v_* is a characteristic velocity and v is again the three-dimensional velocity.

From the results of a Kolmogorov-Smirnov test, they concluded that the Maxwellian model is the least favoured. On the other hand, they disfavour also the bimodal distribution since the bimodality could arise from an attempt to reproduce a non-Maxwellian distribution with a superposition of Maxwellian functions. According to the same K-S test, the single-parameters models described in this Chapter are equally capable to reproduce the observed distribution of pulsar birth velocities.

To explore the effects of the birth velocities on the final phase-space distribution of neutron stars, I adopt the Maxwellian model of Hobbs et al., as well as four of the models proposed by Faucher-Giguère & Kaspi that is the bimodal, the double-sided exponential, the Lorentzian and that of Paczynski. From here on I refer to these models as A, B, C, D and E respectively. The value of the parameters adopted for each velocity distributions, together with the resulting mean three-dimensional velocity, are listed on Table 2. Mean velocities are calculated numerically from simulated velocity vectors. All velocity distributions refer to the frame at rest with the progenitors.

The motion of massive stars can be decomposed in a bulk component given by the circular motion of the Galactic disk, $v_{circ} \sim 200\,\mathrm{km\,s^{-1}}$, and by

a random motion with dispersion $\sigma \sim 25\,\mathrm{km\,s^{-1}}$ with respect to the frame corotating with the disk. These random motion are small if compared with the circular velocity or the birth velocities of neutron stars. Thus, the random motions of progenitors are neglected and the initial velocities of simulated neutron stars are given by vector sum of the birth velocity and the circular velocity at the birthplace, $\mathbf{v} = \mathbf{v}_{birth} + \mathbf{v}_{circ}$.

2.1.3 Gravitational potential

Once the initial conditions have been assigned, the motion of each neutron star in the Galactic potential is described by the equation

$$\ddot{\mathbf{r}} = -\nabla\Phi\,, \tag{2.11}$$

where $\mathbf{r} = \mathbf{r}(R, \phi, z)$ is the position of the neutron star and Φ is the gravitational potential of the Milky Way. I adopt the three-component model proposed by Smith et al. (2007)

$$\Phi = \Phi_B + \Phi_D + \Phi_H\,, \tag{2.12}$$

where Φ_B, Φ_D and Φ_H represent the contributions from the bulge, disk and dark matter halo, respectively. The gravitational potential of the bulge is (Hernquist, 1990)

$$\Phi_B = -\frac{GM_B}{r + r_B}\,, \tag{2.13}$$

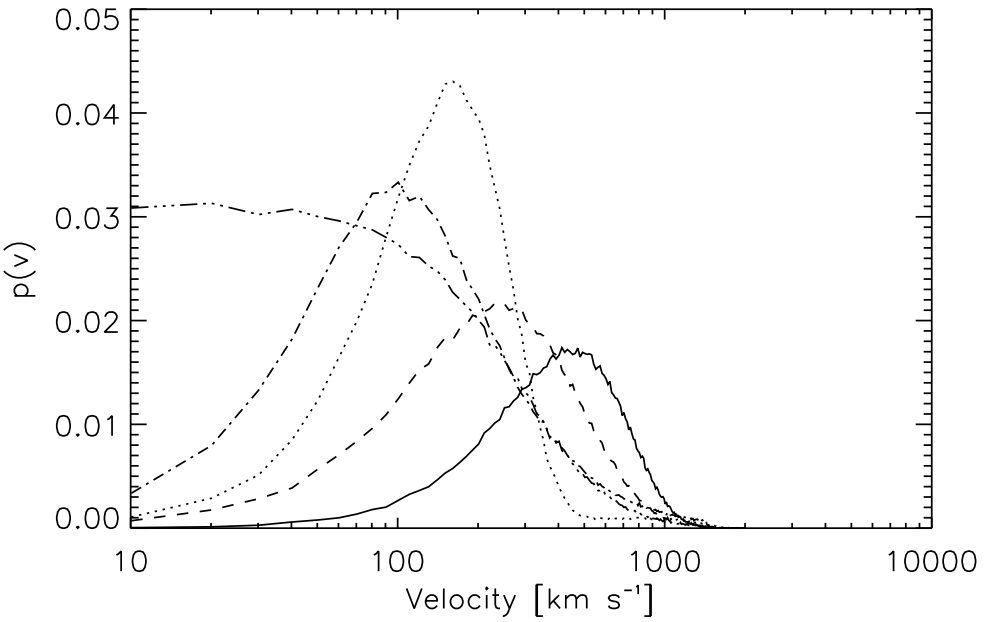

Figure 5: Differential velocity distributions obtained from Monte Carlo simulations of velocitiy vectors. Line style represent models A (solid), B (dotted), C (dashed), D (dot-dashed) and E (triple dot-dashed).

Table 2: Velocity distribution models. $\langle v \rangle$ represents the aritmethic mean, calculated from Monte Carlo simulations of velocity vectors.

Model	Parameters	$\langle v \rangle$ $[\mathrm{km\,s^{-1}}]$
A	$\sigma = 265\,\mathrm{km\,s^{-1}}$	420
B	$\sigma_1 = 160\,\mathrm{km\,s^{-1}}$ $\sigma_2 = 780\,\mathrm{km\,s^{-1}}$ $w = 0.9$	335
C	$v_{exp} = 180\,\mathrm{km\,s^{-1}}$	400
D	$\gamma = 100\,\mathrm{km\,s^{-1}}$	447
E	$v_* = 560\,\mathrm{km\,s^{-1}}$	331

where $M_B = 1.6 \times 10^{10}\, M_\odot$ and $r_B = 0.6$ kpc are respectively the mass and the scale-radius of the bulge and $r = \sqrt{R^2 + z^2}$ is the distance from the Galactic center. The gravitational potential of the disk is (Miyamoto & Nagai, 1975)

$$\Phi_D = -\frac{GM_D}{\sqrt{\left\{R^2 + \left[R_D + \sqrt{z_D^2 + z^2}\right]^2\right\}}}, \tag{2.14}$$

where $M_D = 5 \times 10^{10}\, M_\odot$ is the mass of the disk and the $R_D = 4$ kpc and $z_D = 0.3$ kpc are respectively the scale length and scale height of the disk. Finally, the potential of the dark matter halo is (Navarro et al., 1996)

$$\Phi_H = -\frac{4\pi\, G\rho_s r_{vir}^3}{c^3 r} \log\left(1 + \frac{c\, r}{r_{vir}}\right), \tag{2.15}$$

where

$$\rho_s = \frac{\rho_{cr}\Omega_0\delta_{th}}{3} \frac{c^3}{\ln(1+c) - c/(1+c)} \tag{2.16}$$

is the characteristic density, c is the concentration parameter, r_{vir} is the virial radius and ρ_{cr} is the critical density of the Universe.

The parameters of potential are taken from Smith et al., except for the concentration parameter c and the virial radius r_{vir} (19.2 and 274 kpc respectively), which were adjusted to match the standard values of the International Astronomical Union for the distance of the Sun from the Galactic center, $R_0 = 8.5\,$kpc, and the circular velocity at the solar circle, $v_{circ}(R_0) =$

$220\,\mathrm{km\,s^{-1}}$. The escape velocity at the solar radius, $v_{esc}(R_0) \simeq 544\,\mathrm{km\,s^{-1}}$ is also taken from Smith et al. The corresponding value of the virial mass is $M_{vir} \sim 10^{12}\,M_\odot$.

Very recently Reid et al. (2009) gave a new estimate of the circular velocity, $v_{circ}(R_0) \simeq 254\,\mathrm{km\,s^{-1}}$ with $R_0 = 8.4\,\mathrm{kpc}$, obtained from proper motions of massive star forming regions. This means that our Galaxy may be more massive that what estimated by e.g. Smith et al. To assess the effect of the enhanced mass of the Galaxy on the orbits of neutron stars, I consider also a model of the potential with a different set of parameters: the masses of the bulge and disk are increased by a factor $(254/220)^2$, that is the ratio of the squared circular velocities in the two cases. For the halo, the concentration parameter c remains the same while the virial radius r_{vir} is in this case $\sim 332\,\mathrm{kpc}$, which yields an ~ 80 percent increase of the virial mass, $M_{vir} \sim 1.8 \times 10^{12}\,M_\odot$.

It should be noted that in the model where $v_{circ}(R_0) = 254\,\mathrm{km\,s^{-1}}$, the escape velocity is $\sim 664\,\mathrm{km\,s^{-1}}$. This is higher than the central value, $544\,\mathrm{km\,s^{-1}}$ estimated by Smith et al. (2007); however, it is not far from their 90% upper limit ($\sim 608\,\mathrm{km\,s^{-1}}$), especially when it is considered that v_{esc} was obtained by assuming $v_{circ} = 220\,\mathrm{km\,s^{-1}}$, and that modifying such assumption introduces further uncertainty in its determination (M. C. Smith, private communication).

2.1.4 Orbit Integration

A run of the simulation, 150000 orbits each, is then launched, one for every combination of radial and birth velocity distributions, assuming constant birth rate during the whole Milky Way life-time. Hence, the age of each neutron star is assigned randomly from an uniform distribution. The orbit

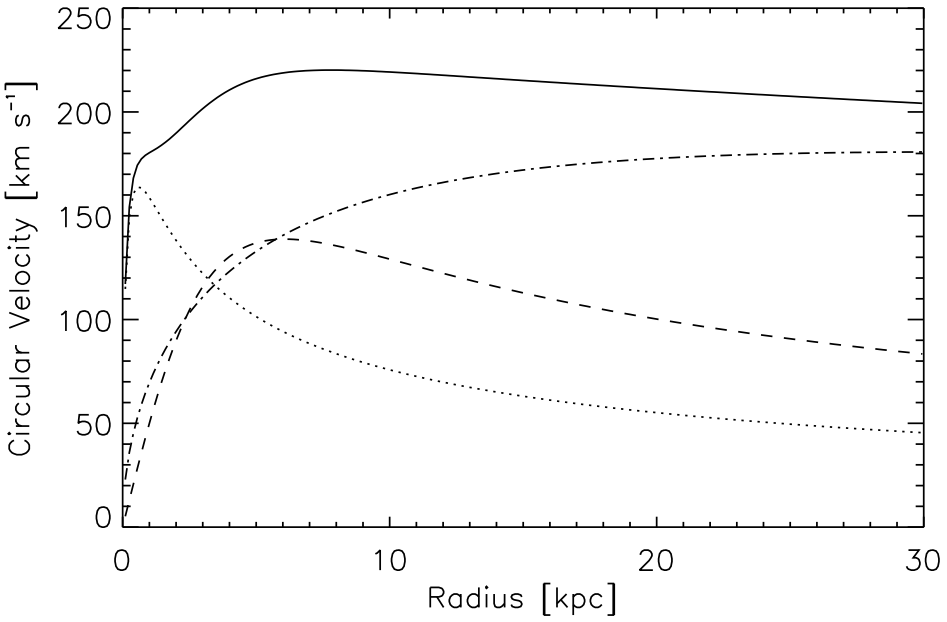

Figure 6: Rotation curve for our Milky Way model (solid). Dotted, dashed and dot-dashed lines represent the bulge, disk and dark matter halo contributions, respectively.

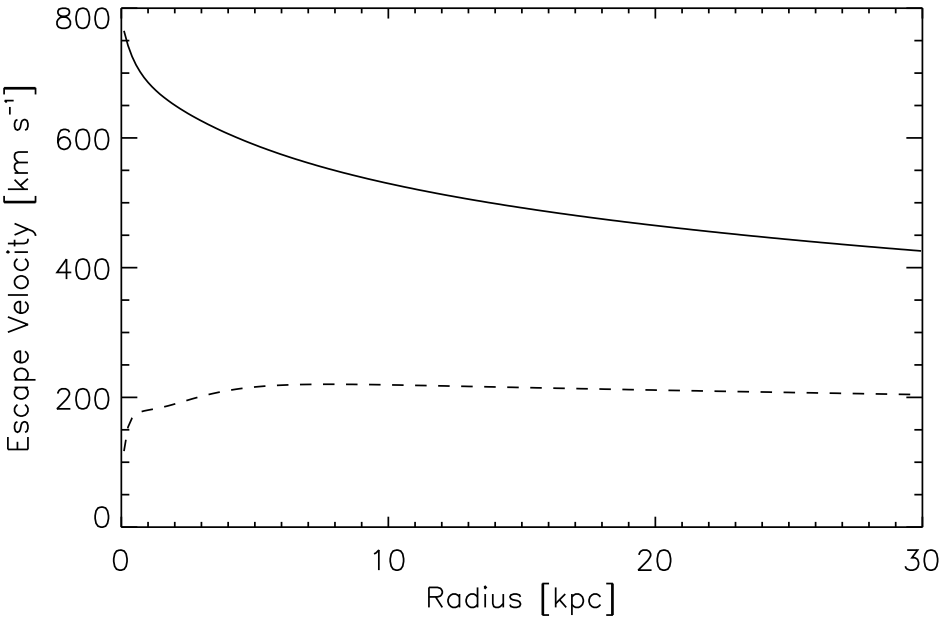

Figure 7: Escape velocity on the Galactic plane as a function of the distance from the Galactic plane. The circular velocity (dashed) is plotted for comparison.

of each neutron star is then integrated numerically, for a time corresponding to its assigned age. The axial symmetry of the potential implies conservation of angular momentum with respect to the axis of rotation of the Galaxy. This allows to reduce the number of equations in the system 2.11 to four

$$\begin{aligned} \frac{dR}{dt} &= v_R\,, \\ \frac{dz}{dt} &= v_z\,, \\ \frac{dv_R}{dt} &= \frac{\partial\Phi}{\partial R} + \frac{j_z^2}{R^3}\,, \\ \frac{dv_z}{dt} &= \frac{\partial\Phi}{\partial z}\,, \end{aligned} \tag{2.17}$$

where j_z is the angular momentum with respect to the z axis. Integration of the systems of equations 2.17 is performed with a 4th order Runge-Kutta algorithm (e.g. Press et al. 1992) with customized adaptive step-size. The relative accuracy of integrations is kept below 10^{-6} using the energy per unit mass E as reference, i.e. $(\delta E/E) \leq 10^{-6}$, where

$$E = \frac{v^2}{2} + \Phi(\mathbf{r})\,. \tag{2.18}$$

To limit the computation time[2] and avoid lock-ups of the code, all neutron stars reaching 0.1 kpc from the Galactic center are discarded. The fraction of neutron stars travelling to within 0.1 kpc from the Galactic center is less than 1 percent in each run.

[2]The CPU time for a typical run is about 1 day.

2.2 Results of the simulation

The results of these simulations suggest that the statistical properties of neutron stars are affected mainly by the distribution of birth velocities, while the effects of different distributions of progenitors are less prominent. Results of models differing only for the distribution of progenitors are quite similar, the main difference is the shape of the surface density towards the inner part of the Galaxy (Figure 8): in fact, in models based on the distribution of progenitors proposed by Paczynski, the density peaks at the Galactic center whereas for other models the density peaks away from the center.

Moreover, it can be argued that the distribution proposed by Paczynski, in spite of being obtained from observations of external galaxies, may better represent the long-term star formation history of our Milky Way. The other models are based on the present-day distribution of population I objects, which could have been rather different in past epochs (see e.g. Chiappini et al., 2001) and are thus better suited for population studies of young/middle-aged neutron stars (like radio pulsars or magnetars). For this reason I focus on results of models 1A to 1E, i.e. with the distribution of progenitors of Paczynski.

2.2.1 Fraction of bound neutron stars

I first compute the fraction of neutron stars in bound orbits, f_{bound}. Neglecting all those processes that could alter its energetic state (e.g. N-body interactions or scattering by molecular clouds and Galactic spiral arms), the final fate of a neutron star is known once its initial position and velocity are given. A neutron star is bound when its initial velocity is lower than the escape velocity at the birthplace, $v_i < v_{esc}(\mathbf{r})$, with

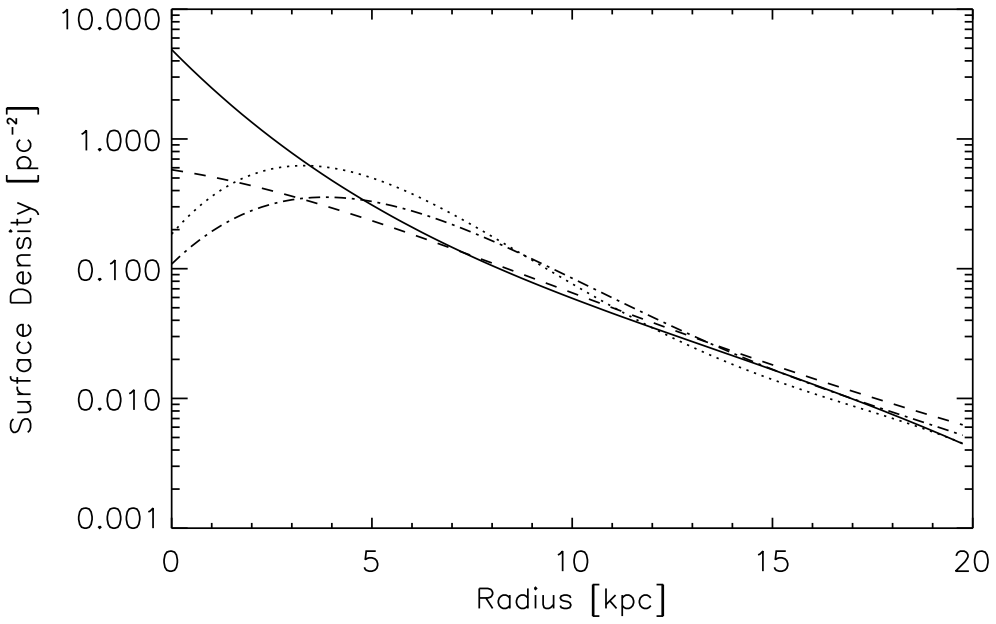

Figure 8: Surface density of neutron stars in the disk, obtained from best fit parameters ($N_{star} = 10^9$). Models 1B (solid line), 2B (dotted), 3B (dashed) and 4B (dot-dashed).

$$v_{esc}(\mathbf{r}_i) = \sqrt{-2\Phi(\mathbf{r}_i)}\,, \tag{2.19}$$

where $\mathbf{r}_i$ is the position of the newborn neutron star. Thus

$$f_{bound} = \frac{N(v < v_{esc})}{N_{star}}\,. \tag{2.20}$$

The retention fraction is ~ 0.7 for models 1A, 1C and 1D, while for models 1B and 1E, $f_{bound} \sim 0.9$ and 0.8 respectively (Table 3).

2.2.2 Distribution of heights

To model the distribution of height on the Galactic plane, I adopt a logistic function (see e.g. Fig. 9)

$$f(z) = \frac{1}{(b_0 b_1^z + b_2)}\,, \tag{2.21}$$

From these fits I estimate the average half-density half-thickness $z_{1/2}$ of the disk neutron stars (Table 3). The values of the coefficients of the fit for each model, together with the corresponding maximum error, are listed in the Appendix (Table 11). The half-density half-thickness shows substantial variations from model to model, going from ~ 100 to $\sim 400\,$pc for models 1A to 1D. For model 1E in particular, $z_{1/2} \sim 30\,$pc, i.e. roughly an order of magnitude smaller than those obtained from other models. I will return on this fact later.

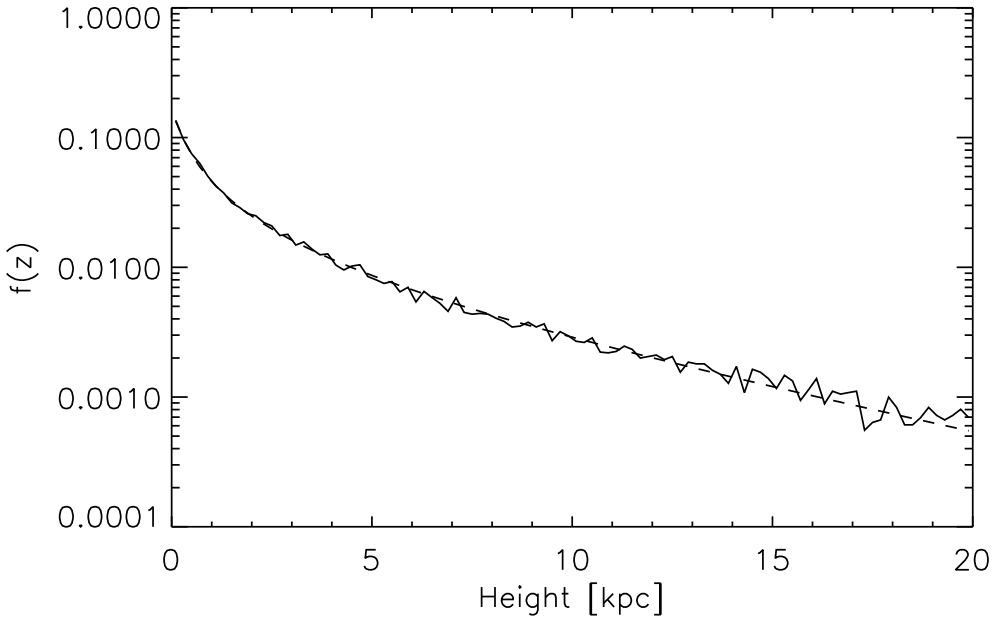

Figure 9: Distribution of heights *f(z)* - Model 1A. Dashed line represents the fitting function.

2.2.3 Neutron stars in the disk

Here I define the Galactic disk as the cylindrical volume with radius 20 kpc and height 0.4 kpc, that is $R \leq 20$ kpc and $|z| \leq 0.2$ kpc. The fraction of neutron stars that reside in the disk, f_{disk}, goes from $\sim$ 0.05 to $\sim$ 0.20. Hence, the majority of neutron stars born in the disk of Milky Way, even those in bound orbits, do not reside in it (see Table 3).

I fit the logarithmic surface density of the disk adopting a fourth order polynomial as fitting function

$$\log \Sigma(R) = a_0 + a_1 R + a_2 R^2 + a_3 R^3 + a_4 R^4 \, . \tag{2.22}$$

The values of the coefficients a_j are listed in the Appendix (Table 10).

I made a visual check of the final distribution of neutron stars in the disk, looking for traces of the spiral arms. I found no evidence of spiral structure in the evolved distribution (compare Figs. 4 and 10).

2.2.4 Mean velocities

The mean velocity of neutron stars in the disk, calculated in the reference frame at rest with respect to the Galactic center, is roughly the same for all models, $\langle v \rangle \sim 210 - 230\,\mathrm{km\,s^{-1}}$, while in the frame corotating with the disk the mean velocity is lower, $\langle v^{LSR} \rangle \sim 150 - 190\,\mathrm{km\,s^{-1}}$. An exception are models based on the velocity distribution E, which show mean velocities in the corotating frame of $\sim 80\,\mathrm{km\,s^{-1}}$. This fact can be easily explained: in the E model low birth velocities have higher probability (see Figure 5) and

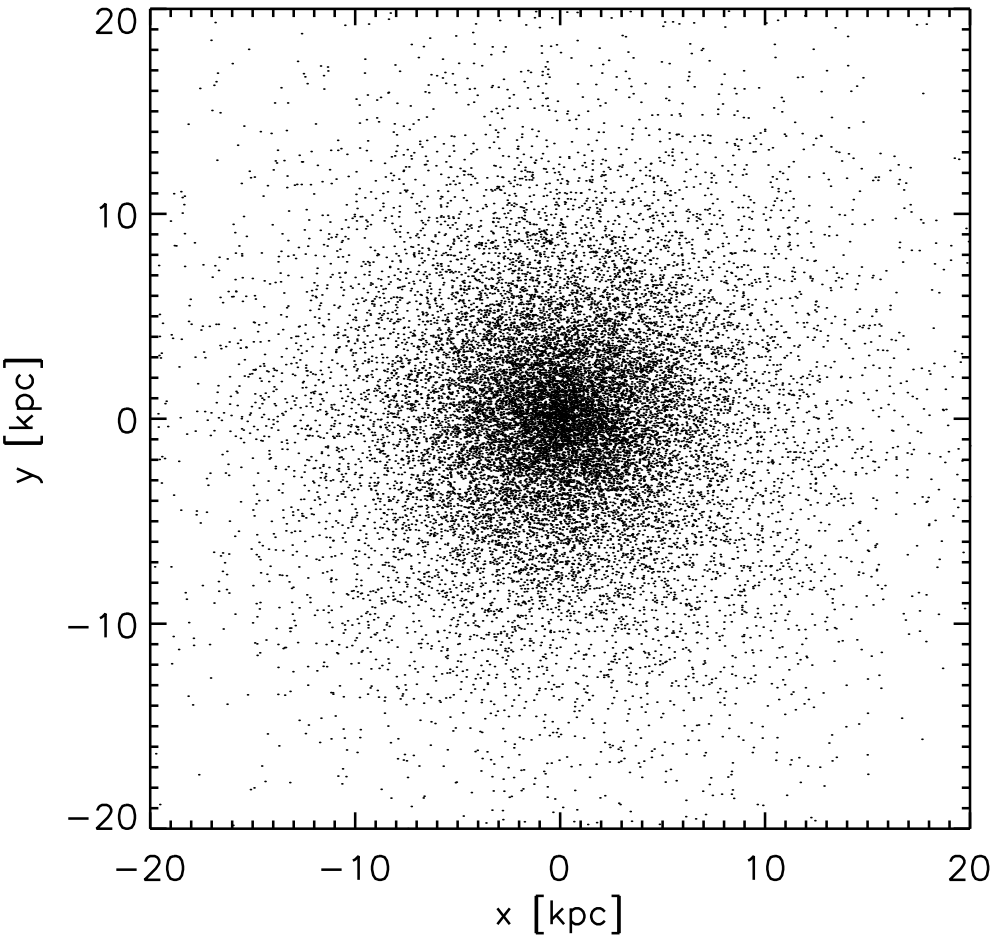

Figure 10: Final distribution of neutron stars in the disk - Model 1E*.

Table 3: Statistical properties of neutron stars in the disk.

Model	1A	1B	1C	1D	1E	1A*	1B*	1C*	1D*	1E*
f_{bound}	0.70	0.88	0.72	0.71	0.79	0.84	0.91	0.82	0.77	0.85
f_{disk}	0.05	0.11	0.10	0.12	0.19	0.06	0.13	0.12	0.16	0.21
$z_{1/2}$ [pc]	367	225	164	100	33	345	192	149	80	28
$\langle v \rangle$ [$\mathrm{km\,s^{-1}}$]	230	220	215	213	213	262	250	249	245	245
$\langle v^{LSR} \rangle$ [$\mathrm{km\,s^{-1}}$]	180	146	199	164	82	199	156	216	176	89
$f_{v<50\,\mathrm{km\,s^{-1}}}$ [%]	< 1	< 1	< 1	< 1	< 1	< 1	< 1	< 1	< 1	< 1
$f^{LSR}_{v<50\,\mathrm{km\,s^{-1}}}$ [%]	1.9	6.0	3.3	7.4	43.7	1.4	3.9	2.9	6.8	37.9

thus the main contributor to the velocity of the star is the circular velocity, $\mathbf{v}_{birth} + \mathbf{v}_{circ} \simeq \mathbf{v}_{circ}$.

The low velocity in the local standard of rest implies also that neutron stars can not move too far away from the disk and that is the reason why the scale height is considerably lower than in other models.

Following Zane et al. (1995), the cumulative velocity distribution of neutron stars with respect to the Galactic center and the corotating frame are fitted with the function

$$G(v) = \frac{\left(v/v_0\right)^m}{1 + \left(v/v_0\right)^n}\,, \tag{2.23}$$

where a v_0 is a characteristic velocity. Fit values for v_0, m and n are listed in the Appendix (Table 12).

2.2.5 The solar neighbourhood

To compare my results with previous studies, e.g. Blaes & Madau (1993) and Zane et al. (1995), I focus now on the statistical properties of neutron stars; in the so-called solar region, $7.5 \leq R \leq 9.5$ kpc.

The local surface density Σ_0 varies from ~ 0.4 to $2 \times 10^5\, N_9\, \mathrm{kpc}^{-2}$, where N_9 is the total number of neutron stars born in the Galaxy, expressed in units of 10^9. The spatial density of neutron stars in the solar vicinity, n_0, also varies by a factor ~ 5 between models, from ~ 1 to $5 \times 10^{-4}\, N_9\, \mathrm{pc}^{-3}$.

Thus, up to $\sim 10^3$ neutron stars should be harboured in the Local Bubble, a region of very low density, $n \sim 0.07\, \mathrm{cm}^{-3}$, nearly centered at Sun and with radius ~ 100 parsec. The distance of the nearest neutron star is therefore

$$d_{min} \sim \left(\frac{3}{4\,\pi\,n_0}\right)^{1/3} \sim 10\,\mathrm{pc}\,. \tag{2.24}$$

2.2.6 Neutron stars in the halo

Bound neutron stars in the halo can reach distances as large as $\sim 1\,\mathrm{Mpc}$ from the Galactic center, however the majority lies within the virial radius of the Milky Way ($\sim 270\,\mathrm{kpc}$). Unbound neutron stars become dominant at $\sim 500\,\mathrm{kpc}$ (Figure 11) and can travel much farther away than bound neutron stars, because their velocity is only weakly affected by the gravitational field of the Galaxy. Accordingly, the mean velocity of neutron stars in the halo begins to rise from $\sim 500\,\mathrm{kpc}$.

2.2.7 Sky density of neutron stars

I compute the projected number density of neutron stars in heliocentric coordinates (l,b,d) for objects within 10 kpc from the Sun. The resulting map of the sky density is shown in Figure 12. It is evident that most neutron stars cluster in the region of the Galactic bulge, where the density is several times 10^3 to $10^4\,N_9\,\mathrm{deg}^{-2}$, depending on the model.

Since most neutron stars are in the halo, it can be expected that the sky density is non-negligible even at high Galactic latitudes, in particular considering also neutron stars at large distance. Hence, I compute also the expected density of neutron stars in the direction of the Magellanic Clouds, assuming distances of 48 and 61 kpc for the Large and Small Magellanic Cloud, respectively. The sky density is $\sim 2-3\,\times 10^2\,N_9\,\mathrm{deg}^{-2}$ towards both directions.

Table 4: Statistical properties of neutron stars at the solar circle.

Model	1A	1B	1C	1D	1E	1A*	1B*	1C*	1D*	1E*
Σ_0 $[10^5\, N_9\, \mathrm{kpc}^{-2}]$	0.44	1.02	0.90	1.21	1.93	0.63	1.31	1.17	1.55	2.33
n_0 $[10^{-4}\, N_9\, \mathrm{pc}^{-3}]$	1.1	2.6	2.3	3.0	4.8	1.6	3.3	2.9	3.9	5.8
d_{min} [pc]	12.9	9.8	10.2	9.2	7.8	11.5	9.0	9.3	8.5	7.4
$\langle v \rangle$ $[\mathrm{km\,s}^{-1}]$	216	213	204	206	216	248	242	234	238	249
$\langle v^{LSR} \rangle$ $[\mathrm{km\,s}^{-1}]$	173	140	191	158	72	191	150	203	167	79
$f_{v \leq 50\, km\, s^{-1}}$ [%]	< 1	< 1	< 1	< 1	< 1	< 1	< 1	< 1	< 1	< 1
$f^{LSR}_{v \leq 50\, km\, s^{-1}}$ [%]	2.5	4.3	3.5	8.4	49.7	1.4	3.2	3.4	7.8	45.4

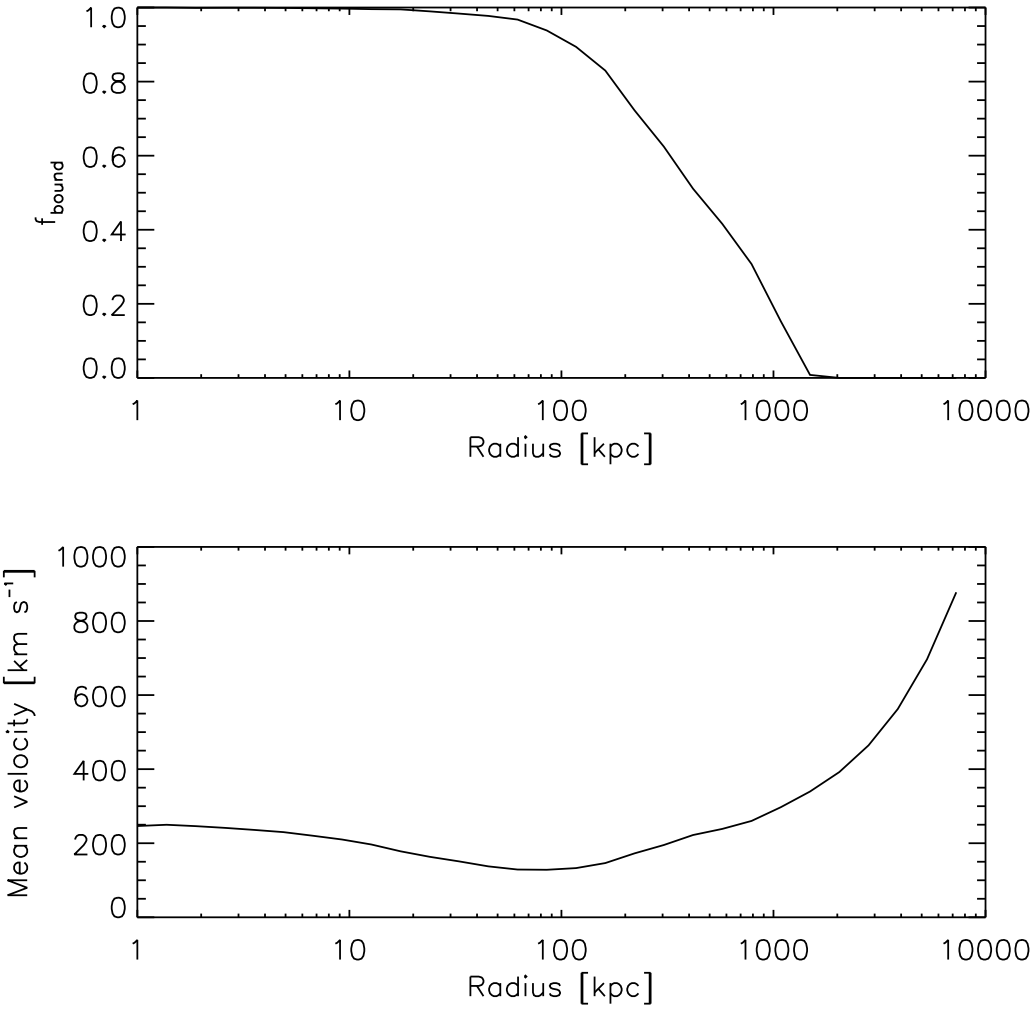

Figure 11: Fraction of bound NSs (top) and mean velocity of NSs (bottom) as a function of the Galactocentric radius.

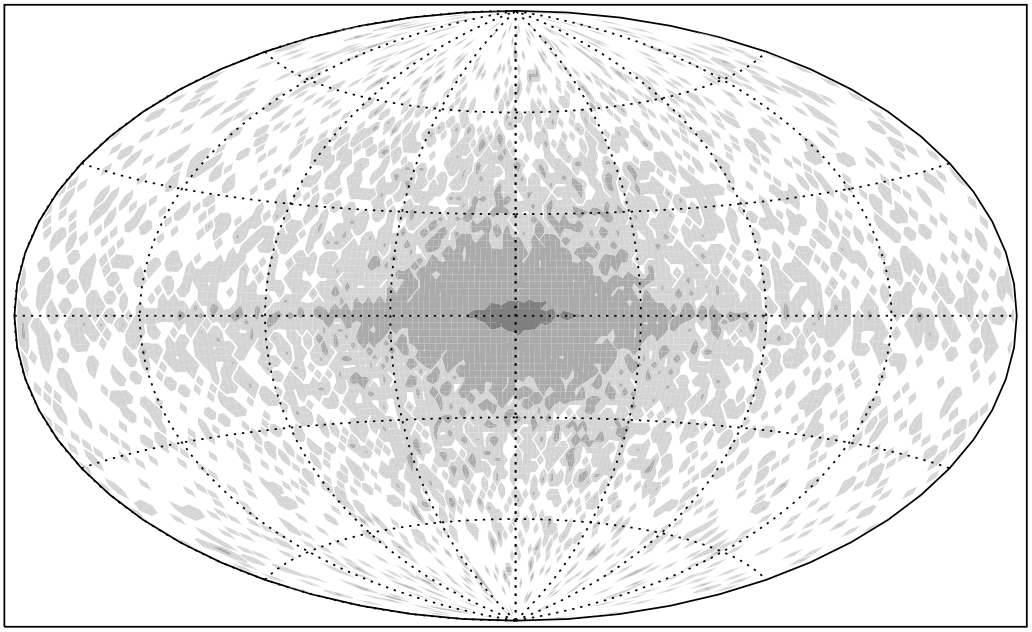

Figure 12: Aitoff projection of the sky density of neutron stars for objects within 10 kpc from the Sun (model 1A). Contour levels are drawn at $10, 10^2, 10^3\,\mathrm{deg}^{-2}$, respectively. The patchy appearance is due to poissonian noise.

2.2.8 Results with different potential

Calculations made with the updated potential are labelled with an asterisk in the tables and give the following results. The retention fraction f_{bound} exhibits a significant increase, especially for models 1A* and 1C*, while for the remaining ones the enhancement is less conspicuous. In all cases the fraction of neutron stars retained by the disk is only slightly increased (Table 3).

In all models with the updated potential, the scale height of the population is lower due to the increased masses of the disk and bulge, the decrease in $z_{1/2}$ being of the order of 10 - 20 percent (see Table 3).

The higher number of neutron stars retained by the disk implies also higher values of the surface and volume densities, together with the projected density towards the Galactic plane. For the same reason, even relatively fast neutron stars can be found in the disk, thus increasing the mean velocity of this population (see Tables 3 and 4).

2.3 Summary of the results

The results of these numerical simulations show that the distribution of birth velocities is the main factor driving the dynamics of neutron stars in the Milky Way. I obtain substantially different values of f_{bound} among different birth velocity models, with the shape of the distribution (position of the peak, bimodality, etc.) also playing a role in determining the final fate of bound neutron stars.

The highest escape fraction, ~ 0.3, are obtained with models A, C and D. This value is lower than that found by e.g. Arzoumanian et al. and similar to that inferred by Hobbs et al.. This is probably due to the different

models of the distribution of free electrons adopted to estimate the distance of radio pulsars. Arzoumanian et al. adopted the model of Taylor & Cordes (1993). Both Hobbs et al. and Faucher-Giguère & Kaspi adopted instead the revised model of Cordes & Lazio (2002), which reduced distance estimates, and thus also velocities, of young pulsars. As a consistency check, I performed a simulation run with the distribution of velocities proposed by Arzoumanian et al., obtaining $f_{bound} \sim 0.54$, confirming my hypothesis. The adoption of a different potential, with higher mass of the Galaxy, implies higher escape velocities. Hence, only the fastest neutron stars, $\sim 10 - 15$ percent, can definitely escape from the Milky Way.

Albeit more than 70 percent of the neutron stars born in the Milky Way are in bound orbits, the present-day number of neutron stars in the disk is only a minor fraction of the total, $\lesssim 0.20$. The remaining ones are found in the halo where they spend most of their life. Even so, the ratio of young, $t \lesssim 10^7$ years, to old neutron stars in the disk is very low: for each neutron star detected as a young active source there should be still more than 100 old objects.

Simulated neutron stars are born with significantly higher velocities with respect to what is found in other works. In spite of this, the resulting half-density at half-thickness shows no significant differences with previous studies. Also, the local spatial density of neutron stars falls between those found by e.g. Blaes & Madau and Zane et al. (1995) that found by Paczynski (1990), i.e. approximately between ~ 1 and $\sim 5 \times 10^{-4}\, N_9\, \mathrm{pc}^{-3}$. This means that the nearest neutron star lies within ~ 10 parsec from the Sun.

The mean velocity is higher by at least a factor ~ 2 with respect to, for example, that found by Blaes & Madau and Zane et al. Low velocity neutron stars ($v \leq 50\,\mathrm{km\,s^{-1}}$) in the disk are a tiny fraction, $f_{v \leq 50\, km\, s^{-1}} < 1\%$. This

fraction is instead $f^{LSR}_{v\leq 50\,km\,s^{-1}} \sim 5\%$, in the reference frame corotating with the Galactic disk.

Most of Galactic neutron stars, either bound and unbound, run away from the Galactic plane in a short timescale and form a halo which extends well beyond the virial radius of the Milky Way. The (spherical) radial distribution of halo neutron stars clearly shows a separation between bound and unbound objects. Unbound neutron stars become dominant at $r \sim 500$ kpc.

The results reported in this Chapter have been published in Sartore et al. (2010). I stress that these results do not account for neutron stars generated in the bulge wich, as I will show in the next Chapter, may account for $\sim$ half of the neutron stars born in the Galaxy.

3 MICROLENSING FROM ISOLATED NEUTRON STARS AND BLACK HOLES

As shown in the previous Chapter, the observability of old isolated neutron stars and black holes as sources accreting from the interstellar medium is still controversial. However, they certainly can still act as gravitational lenses.

3.1 The microlensing phenomenon

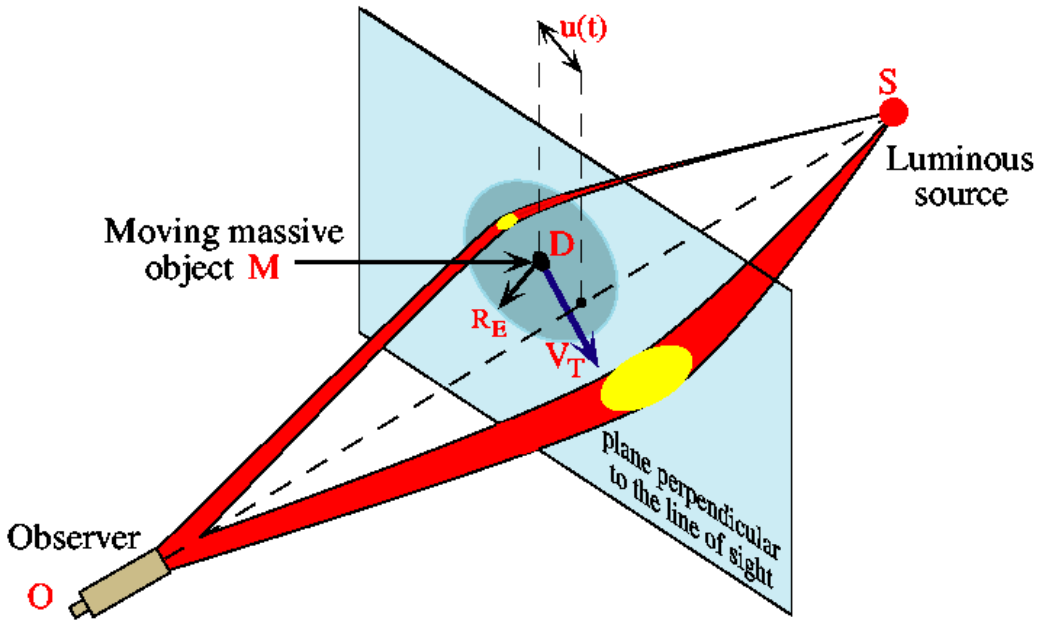

Figure 13: Sketch model of a microlensing event. Source: Moniez (2010).

The phenomenon of gravitational microlensing, that is the deflection and amplification of the light of a star by a foreground massive object, has been first predicted by Einstein (1936), but the prospects of observing such kind of events were, according to him, negligible.

Gravitational microlensing was seriously reconsidered in a series of seminal papers by Paczynski (1986, 1991), in order to detect massive objects in the Galactic halo and bulge, and thus to constrain the nature of the dark matter within the halo itself. To this purpose, several survey programs have been started, like the MACHO (MAssive Compact Halo Objects, e.g. Alcock et al., 1993), the OGLE (Optical Gravitational Lensing Experiment, e.g. Udalski et al., 1992), the EROS (Experiènce de Recherche d'Objects Sombres, e.g. Aubourg et al., 1993) and the later MOA (Microlensing Observations in Astrophysics, e.g. Muraki et al., 1999) projects. These surveys have been very successful in detecting events towards the Magellanic Clouds, the Galactic spiral arms and in particular the Galactic bulge, for which the number of events detected surpasses by far all the others (see e.g. Moniez, 2010, for a review).

Since the rate of microlensing events depends on the density of both source and lense objects, and considering that the sky density of neutron stars, like that of normal stars, also peaks towards the Galactic bulge (Figure 12), its is straightforward to think that this is the most suitable direction where to detect candidate neutron star and black hole lenses. Thus I limit the study to the contribution of neutron stars and black holes to the microlensing rate towards the Galactic bulge. This contribution must be compared to that of other, more numerous, stellar populations in the Galaxy.

The first theoretical predictions of the microlensing optical depth (τ, see Chapter 3.2 for a definition) towards the bulge inferred values of $\sim 0.5 - 0.8 \times 10^{-6}$ (Paczynski, 1991; Griest, 1991) for the luminous stellar component of the Milky Way. The initial measurements of the optical depth returned significantly larger values, e.g. $\tau = 3.3 \times 10^{-6}$ (Udalski et al., 1994)

and $\tau = 3.9 \times 10^{-6}$ (Alcock et al., 1997), respectively. To explain this discrepancy, Kiraga & Paczynski (1994) suggested that the Galactic bulge could give a substantial contribution to the optical depth. Hence, they included this contribution in their calculations. Theoretical estimates with these new models agree well with the more recent measurements of the optical depth, $\tau = 2.17 \times 10^{-6}$ (Popowski et al., 2005, MACHO), $\tau = 2.55 \times 10^{-6}$ (Sumi et al., 2006, OGLE) and $\tau = 1.62 \times 10^{-6}$ (Hamadache et al., 2006, EROS).

The contribution of neutron stars and black holes to microlensing has been estimated by Gould (2000); Wood & Mao (2005); Calchi Novati et al. (2008). These authors found that $\sim 2-3$ percent of the events are related to neutron stars and black holes. However, they did not take into account that these objects have a different phase space distribution with respect to normal stars, because of the large kick velocities received at birth (e.g. Hobbs et al., 2005; Gualandris et al., 2005). This fact has two opposite effects. First, the velocities at birth can be higher than the escape velocity from the Galaxy. Hence, a non negligible fraction of remnants may have escaped from the Galaxy and thus cannot contribute to the microlensing rate towards the bulge. Second, the larger velocities imply a higher rate of events than what expected from a similar population of lenses moving at lower speeds, as showed by Griest (1991).

3.2 Basic theory of microlensing

A microlensing event occurs when a massive compact object passes near-by the line-of-sight (l.o.s. hereafter) of a source star, producing non-resolved and amplified images of it. Assuming point-like source and lens and constant relative speed between the two, the light curve of the event follows the law

$$A(t) = \frac{u(t)+2}{u(t)\sqrt{u(t)^2+4}}\,, \tag{3.1}$$

where $A(t)$ is the amplification factor of the source's light and $u(t)$ is the projection of the distance between the source and lens in the plane of the sky, in units of the Einstein radius (Griest, 1991)

$$R_E = 2\left[\frac{G\,M}{c^2}\,\frac{D_l\,(D_s - D_l)}{D_s}\,\right]^{1/2} = 1.38\,\times 10^{-8}\left[m\,D_s\,x\,(1-x)\right]^{1/2}\,\mathrm{kpc}\,, \tag{3.2}$$

where M is the mass of the lens, D_s is the source-observer distance, D_l is the lens-observer distance, $x = D_l/D_s$ and $m = M\,/\,M_\odot$ is the mass of the lens in solar units. The probability that a background source is lensed at any given time is called optical depth for microlensing (Vietri & Ostriker, 1983) and it depends on the distribution of lensing matter along the l.o.s. (e.g. Kiraga & Paczynski, 1994; Jetzer et al., 2002).

$$\tau(D_s) = \frac{4\,\pi\,G}{c^2}\int_0^{D_s}\rho_l(D_l)\frac{D_l(D_s-D_l)}{D_s}\mathrm{d}D_l\,, \tag{3.3}$$

where ρ_l is the mass density of the lenses, If both lenses and sources are distributed along the l.o.s., Equation 3.3 becomes

$$\tau = \frac{4\,\pi\,G}{c^2\,I}\int_0^{D_{max}}\tau(D_s)\,\rho_s(D_s)\,D_s^2\,\mathrm{d}D_s\,, \tag{3.4}$$

where ρ_s is the mass density of sources and $I = \int_0^{D_{max}} \rho_s(D_s) D_s^2 \mathrm{d}D_s$ is a normalization factor. Throughout this paper I will assume $D_{max} = 12$ kpc in order to include the contribution of the whole bulge. The optical depth can also be defined as (Griest 1991)

$$\tau = \frac{\pi \langle t_E \rangle \Gamma}{2}, \tag{3.5}$$

where Γ is the rate of lenses entering the tube and $\langle t_E \rangle$ is the average time-scale of the observed events. The duration of a single event depends on the mass of the lens and on the geometry of the system (Moniez, 2010)

$$\begin{aligned} t_E &= \frac{R_E}{v_\perp} = \frac{2}{v_\perp} \left[\frac{G\,M}{c^2} \frac{D_l\,(D_s - D_l)}{D_s} \right]^{1/2} \\ &\sim 79 \left(\frac{v_\perp}{100\,\mathrm{km\,s^{-1}}} \right)^{-1} m^{1/2} \left(\frac{D_s}{10\,\mathrm{kpc}} \right)^{1/2} \frac{[x\,(1-x)]^{1/2}}{0.5} \,\mathrm{days}\,, \end{aligned} \tag{3.6}$$

where $v_\perp$ is the relative velocity between source and lens in the plane perpendicular to the l.o.s.. The differential rate of events is (e.g. Jetzer et al., 2002; Calchi Novati et al., 2008).

$$\mathrm{d}\Gamma = \frac{n_l(D_l)\,\mathrm{d}^3 D_l}{\mathrm{d}t} \frac{n_s(D_s)\,D_s^2\,\mathrm{d}D_s}{I} f(\mathbf{v}_\perp)\,\mathrm{d}^2 v_\perp\,, \tag{3.7}$$

where n_l and n_s are the number density of the lenses and the sources along the l.o.s., while $f(\mathbf{v}_\perp)$ is the distribution of the source-lens relative velocities.

3.3 Model of the Galaxy

In order to compare the contribution of neutron stars and black holes to the microlensing rate towards the bulge with that of other stars, the contribution of each stellar population has to be calculated self-consistently. Hereafter I describe a model of the Milky Way which accounts for all populations of lens and source stars. This model is different from the one described in the former Chapter since now the population of bulge-born compact remnants, both neutron stars and black holes, is taken into account.

3.3.1 Distribution of normal stars

First, I model the distribution of normal stars, that is stars with no natal kicks, in both the Galactic bulge and disk. I adopt the same bulge model of Calchi Novati et al., that is a three-axial bulge with an exponential density profile and a major axis that forms an angle $\phi \sim 24^{\circ}$ with the Sun-Galactic center axis (e.g. Stanek et al., 1997). The total mass of the bulge is $\sim 2 \times 10^{10}\, M_{\odot}$. For the disk, I adopt a thin + thick disk model, both described by an exponential density profile

$$\rho_{D_i}(R,z) = \frac{M_{D_i}}{4\,\pi\,(L_i^2 - L_h^2)\,H_i}\left[\exp\left(\frac{R}{L_i}\right) - \exp\left(\frac{R}{L_h}\right)\right]\exp\left(-\frac{|z|}{H_i}\right),\ i = 1,2 \tag{3.8}$$

where the masses of the thin and thick disks are $M_{D_1} \sim 2.5 \times 10^{10}\, M_{\odot}$ and $M_{D_2} \sim 0.5 \times 10^{10}\, M_{\odot}$, the scale-lengths are $L_1 \sim 2.6$ kpc and $L_2 \sim 3.6$ kpc and scale-heights are $H_1 \sim 0.3$ and $H_2 \sim 0.9$ kpc (Robin et al., 2003), respectively. The mass of the thin disk accounts also for the interstellar medium, $M_{ISM} \sim 0.5 \times 10^{10}\, M_{\odot}$. According to Freudenreich (1998), the

stellar disk is holed at its center, the hole being likely produced by orbital resonances in the potential of the barred bulge (Contopoulos et al., 1989). For the scale-length of the hole in both the thin and thick disks I assume $L_h \sim 1.3$ kpc (Picaud & Robin, 2004).

The motion of bulge and disk stars has both bulk and random components. The Galactic bulge does not rotate as a whole like a rigid body but out of a certain radius the bulk velocity flattens (Rich et al., 2007). Thus I assume that the rotation velocity $v_{rot}^{(b)}$ of the bulge grows linearly to $50\,\mathrm{km\,s^{-1}}$ out of a radius of 1 kpc from the Galactic center. Out of this radius, a flat rotation curve is assumed, with $v_{rot}^{(b)} = 50\,\mathrm{km\,s^{-1}}$. For disk stars, I compute the bulk (circular) motion self-consistently from the potential generated by disk and bulge stars. For simplicity, the random motions of bulge and disk stars are assumed isotropic, with dispersions $\sigma_v^{(b)} = 100$ and $\sigma_v^{(d)} = 25\,\mathrm{km\,s^{-1}}$ which reasonably agrees with the values inferred from observations (Calchi Novati et al., 2008, and references therein).

3.3.2 Updated distribution of neutron stars and black holes

In the previous Chapter I studied the dynamics of a population of disk neutron stars born at a constant rate during the Milky Way life-time, assuming a total of 10^9 objects, consistently with chemical abundances observed in the Galaxy. As Ofek (2009) has pointed out, the total number of disk-born neutron stars inferred from the present-day supernova rate and from the star-formation history of the disk is $\lesssim 4 \times 10^8$ (see also Keane & Kramer, 2008, and references therein). To explain this discrepancy, Ofek suggested that the remaining neutron stars have been generated in the bulge.

Because I am dealing with the microlensing rate of compact remnants toward the Galactic bulge, it is straightforward to think that a substantial

contribution can come from bulge-born objects. Thus I run new simulations of orbits, taking into account the the orbits of those neutron stars and black holes born in the bulge.

The total number of compact remnants in the Milky Way can be estimated by following the approach of Gould (2000). I adopt the initial mass function proposed by Kroupa (2001), i.e. a triple power law model

$$\begin{aligned} \frac{\mathrm{d}N}{\mathrm{d}m} \propto m^{-\alpha}\,, \quad & \alpha = 0.3\,, \quad 0.03 \leq m < 0.08 \\ & \alpha = 1.3\,, \quad 0.08 \leq m < 0.5 \\ & \alpha = 2.3\,, \quad 0.50 \leq m < 100\,. \end{aligned} \tag{3.9}$$

From the mass function, I estimate the number and mass fractions of each stellar population, brown dwarfs, main sequence stars, white dwarfs, neutron stars and black holes. I assume that all stars with $m > 1$ have evolved through the remnant phase. This assumption gives only a gross estimate of the number of disk stars that are now white dwarfs ($1 < m < 8$), because not all stars above these mass had yet evolved up to the white dwarf phase. On the other hand, this assumption is well justified for bulge stars, for which the turn-off mass is $\lesssim 1\,M_{\odot}$ (Gould, 2000, and references therein), and in particular for neutron stars and black holes, because the typical lifetime of massive stars is much shorter than the age of the Galaxy. Hence, I assume that stars with $1 < m < 8$ are now white dwarfs, ($m_{WD} = 0.6$), while stars with masses $8 < m < 40$ and $40 < m < 100$ are treated as neutron stars ($m_{NS} = 1.4$) and black holes ($m_{BH} = 10$), respectively. Results are reported in Table 5.

The knowledge of the masses of the bulge and disk and the mass and

Table 5: Number and mass fractions of the different stellar populations.

	BD	MS	WD	NS	BH
number fraction	0.272	0.653	0.065	0.004	0.0004
mass fraction	0.059	0.744	0.157	0.023	0.016

number fractions of neutron stars and black holes allow to estimate the total number of remnants born in the Galaxy. I obtain $N_{NS}^{(b)} \sim 3.3 \times 10^8$, $N_{BH}^{(b)} \sim 3.2 \times 10^7$, $N_{NS}^{(d)} \sim 4.1 \times 10^8$ and $N_{BH}^{(d)} \sim 4.0 \times 10^7$, where the superscripts *(b)* and *(d)* refer to the bulge and disk populations, respectively.

I run numerical simulations as in Chapter 2 to follow the orbits of 2×10^5 bulge-born and 2×10^5 disk-born synthetic neutron stars and black holes. I adopt a revised gravitational potential for both the Galactic bulge and disk, obtained from superposition of Miyamoto and Nagai disks. The associated density profiles are a close approximation of the density profiles assumed for the bulge and disk of the Galaxy (Chapter 3.3.1). The parameters of the dark matter potential are then fine tuned in order to obtain a circular velocity of $\sim 220\,\mathrm{km\,s^{-1}}$ at the solar circle ($R_\odot = 8.5\,\mathrm{kpc}$). The resulting escape velocity at the same radius is $\sim 450\,\mathrm{km\,s^{-1}}$, that is ~ 17 percent lower than what was assumed in the previous Chapter. For simplicity, I assume that the gravitational potential of the bulge is axisymmetric.

The results obtained are then normalized to the corresponding number of objects expected from each population and reported above. The initial conditions for each object are randomly assigned using a Monte Carlo procedure.

The integration time of each orbit depends on the birth location: for the bulge, I assume that all remnants have an age of $\sim$ 10 Gyr, while the age of disk objects are uniformly distributed between 0 and 10 Gyr. In both cases the radial birth probability is proportional to the corresponding density profile of stars. I assume that the bulge and disk can produce remnants up to 3 and 15 kpc, respectively. The vertical birth probabilities are again assumed proportional to the density of normal stars up to 3 kpc for the bulge and up to 1 kpc for the disk. Because the distribution of evolved neutron stars (and black holes) are insensitive to the initial distribution the azimuthal coordinates are uniformly between 0 and $2\,\pi$ in both cases.

As in the previous Chapter, the initial velocity of each synthetic compact remnant is the vector sum of its birth velocity plus the orbital velocity of the progenitor. The orbital velocity of the progenitor is calculated from the gravitational potential. Hereafter I adopt the Maxwellian distribution proposed by Hobbs et al. (2005) with a dispersion $\sigma = 265\,\mathrm{km\,s^{-1}}$ for the natal kicks.

The velocity distribution of black holes is poorly constrained, and it was assumed that these objects have a dispersion of $\sim 40\,\mathrm{km\,s^{-1}}$ (e.g. White & van Paradijs, 1996). However, the discovery of black hole X-ray binaries with high spatial velocities (Mirabel et al., 2001, 2002), suggests a similar birth velocity distribution for both types of remnants. Hence, I assume the same distribution of birth velocities for both neutron stars and black holes. Finally, I also add a random component to the velocity of the progenitors.

3.4 Results

3.4.1 Optical depth

From the results of new simulation runs described previously, I estimate the microlensing optical depth (Equation 3.4) for different l.o.s. towards the Galactic bulge. In particular I consider a $20^\circ \times 20^\circ$ window centered at $(l, b) = (0^\circ, 0^\circ)$, and study the dependence of τ on the Galactic longitude and latitude. I assume 100 percent detection efficiency and do not take into account the effect of interstellar extinction nor do I apply any flux limit on source stars. In this regard, I consider as sources only the stars in the main sequence, because brown and white dwarfs are expectedly too weak to be efficiently monitored by present surveys.

Figures 14 and 15 show the contour plots of the optical depth of normal stars and compact remnants, respectively. For normal stars the optical depth mostly depends on the Galactic latitude, because of the shape of the bulge and the contribution of the disk. On the other hand, the dependence of τ_{star} from the longitude is weaker (compare this figure with Figure 1 of Calchi Novati et al.). The optical depth of neutron stars and black holes instead has a strong dependence on both the longitude and latitude. There is also a noticeable asymmetry with respect to the Galactic center. The maximum of the optical depth is shifted toward negative longitudes, $l \sim -2^\circ$. This behaviour is due to the l.o.s. intercepting the far end of the Galactic bar when looking towards negative longitudes. In this condition the geometry of the source-lens system implies a larger Einstein radius, and hence larger optical depth.

In Table 6 I report the optical depth of normal stars, neutron stars and black holes for several specific l.o.s. in the selected window. The optical

depth of normal stars is, for example, $\tau_{star} \sim 0.94 \times 10^{-6}$ toward the Baade's Window, $(l, b) = (1^\circ, -3^\circ.9)$, while towards $(l, b) = (1^\circ.50, -2^\circ.68)$ and $(l, b) = (1^\circ.50, -2^\circ.75)$ the optical depth is $\sim 1.43 \times 10^{-6}$ and $\sim 1.40 \times 10^{-6}$, respectively. These values agree reasonably well with those found in the literature.

Without accounting for the different kinematic properties, the contribution of neutron stars and black holes would be proportional to the mass fraction of each sub-population. Also, it would not depend on the line of sight. This translates in a contribution of ~ 2.3 and ~ 1.6 percent of the total, for neutron stars and black holes respectively.

When the kinematic effects are considered, the optical depth differs from what expected. The optical depth is slightly lower than the nominal value obtained when the kinematics is not accounted for. Also, I find that the contribution of remnants to the optical depth is mostly due to objects born in the bulge, $\tau^{(b)}/(\tau^{(d)} + \tau^{(b)}) \sim 0.84$, where $\tau^{(b)}$ and $\tau^{(d)}$ are the optical depths of bulge-born and disk-born remnants, respectively. Because of their larger mass, the contribution of black holes is only a factor ~ 1.5 lower of that of neutron stars.

3.4.2 Rate of events and distribution of time-scales

I compute the expected distribution of event time-scales for different l.o.s. towards the bulge. Results for the Galactic center and the Baade's Window are reported in Table 7 as examples. In general, microlensing events are dominated by self-lensing of bulge low mass stars, these events having a typical duration of $\sim 15 - 20$ days. As expected the rate of events drops rapidly away from the plane, because of the decrease in the density of both

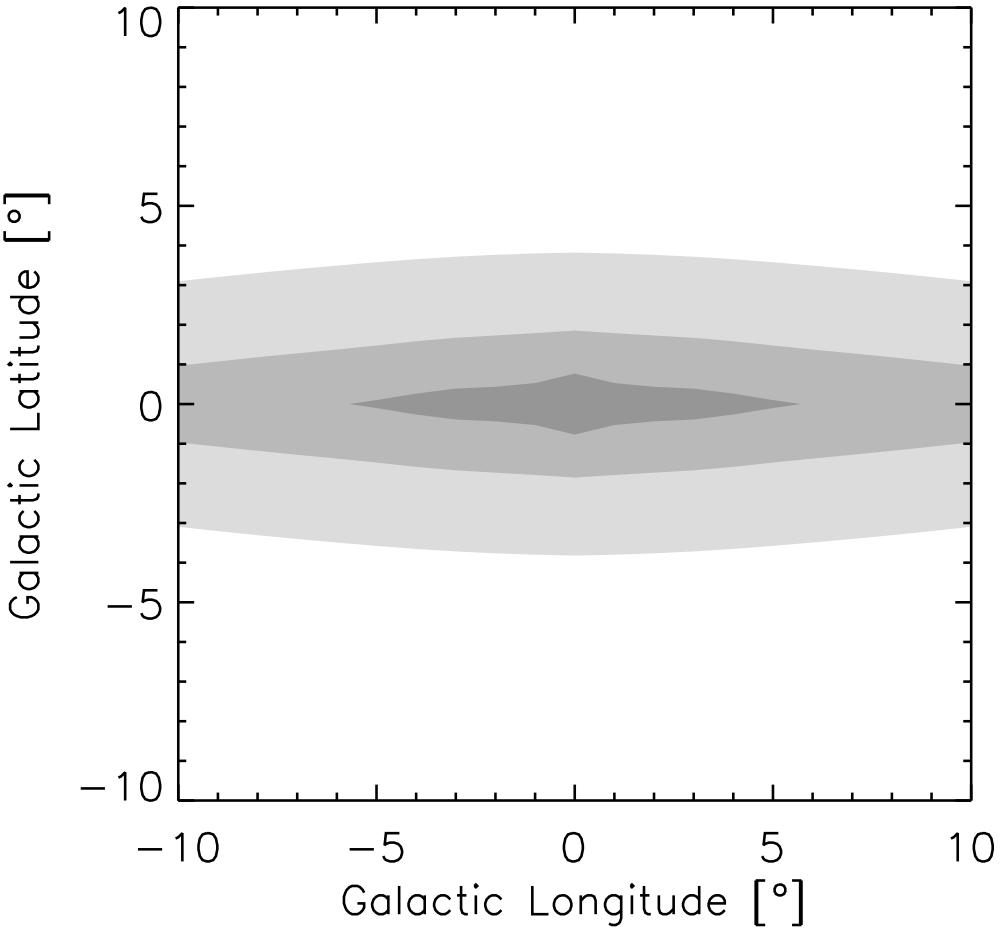

Figure 14: Optical depth profiles of normal stars as a function of the Galactic coordinates. Contour profiles are drawn at $(0.5, 1.0, 2.0, 3.0) \times 10^{-6}$. Darker grey levels indicate larger optical depth.

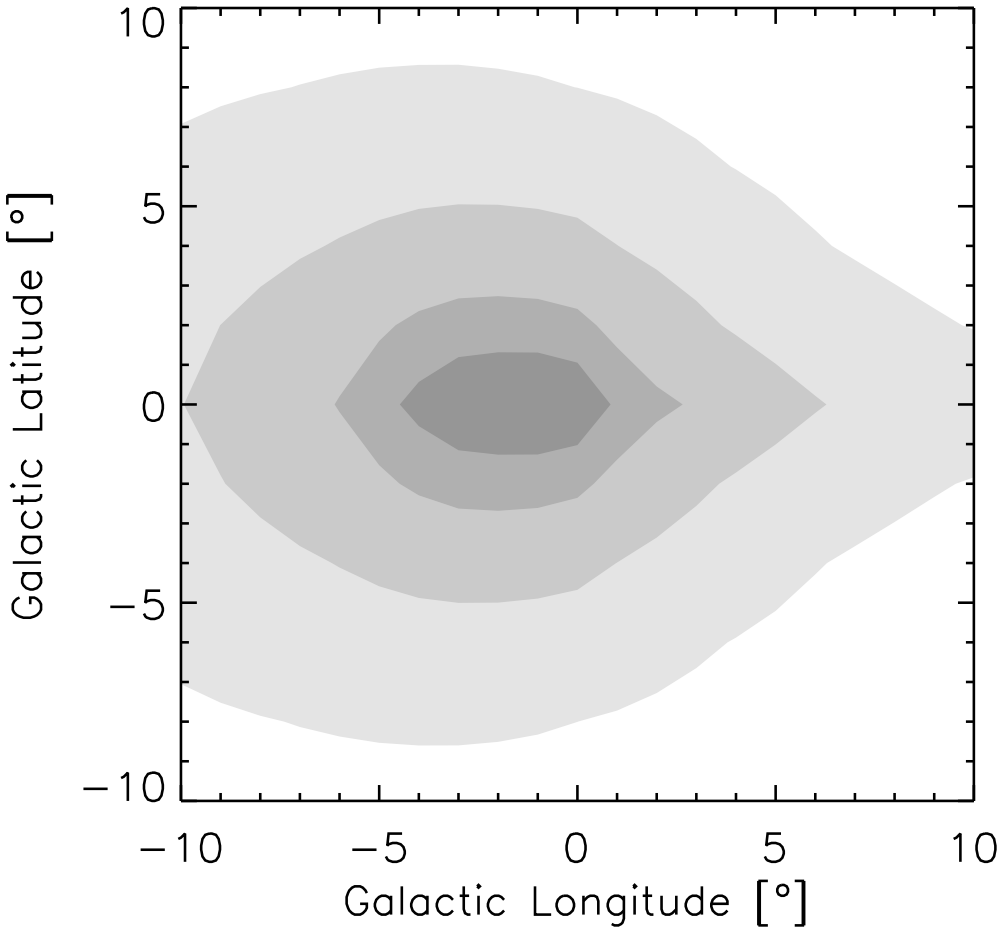

Figure 15: Optical depth profiles of compact remnants as a function of the Galactic coordinates, obtained from sum of the contributions from neutron stars and black holes. Contour profiles are drawn at $(0.5, 1.0, 3.0, 6.0, 8.0) \times 10^{-8}$.

Table 6: Optical depth of normal stars, neutron stars and black holes towards different l.o.s.The superscripts *(b)* and *(d)* refer to the sub-populations of bulge and disk objects, respectively.

l.o.s.	τ_{star}	$\tau_{NS}^{(b)}$	$\tau_{NS}^{(d)}$	$\tau_{BH}^{(b)}$	$\tau_{BH}^{(d)}$
(l, b)	$[\times 10^{-6}]$	$[\times 10^{-8}]$	$[\times 10^{-8}]$	$[\times 10^{-8}]$	$[\times 10^{-8}]$
$(1^\circ, -3^\circ.9)$	0.94	1.51	0.31	1.05	0.21
$(1^\circ.5, -2^\circ.68)$	1.43	1.97	0.38	1.36	0.27
$(1^\circ.5, -2^\circ.75)$	1.40	1.93	0.37	1.33	0.26

sources and lenses. The relative contribution of compact remnants is however increased with respect to the case with no kinematic effects. Indeed, I find that the overall contribution of neutron stars rises from ~ 1 to ~ 5 percent, while for black holes it becomes ~ 1 percent instead of ~ 0.2 percent.

The average duration of the events associated with remnants is lower by a factor ~ 1.5, owing to the large velocities of these objects. The average time-scale of the events is $\langle t_E \rangle \sim 25$ days instead of ~ 36 days for neutron stars, while for black holes $\langle t_E \rangle \sim 67$ instead of ~ 95 days.

Intriguingly, the relative contribution of black holes increases with the time scale. For events with duration longer than 100 days, this contribution is ~ 40 percent (see Figure 8), while neutron stars account for ~ 10 percent of the events.

Table 7: Rates of events and average time-scales toward the Galactic center and the Baade's window.

	l.o.s.	
	$(0^\circ, 0^\circ)$	$(1^\circ, -3^\circ.9)$
Γ_{star} $[\times 10^{-5}\,\mathrm{star}^{-1}\,\mathrm{yr}^{-1}]$	2.67	0.52
$\langle t_E \rangle_{star}$ [days]	16	20
Γ_{NS} $[\times 10^{-6}\,\mathrm{star}^{-1}\,\mathrm{yr}^{-1}]$	1.47	0.40
$\langle t_E \rangle_{NS}$ [days]	25	28
Γ_{BH} $[\times 10^{-6}\,\mathrm{star}^{-1}\,\mathrm{yr}^{-1}]$	0.38	0.10
$\langle t_E \rangle_{BH}$ [days]	67	77

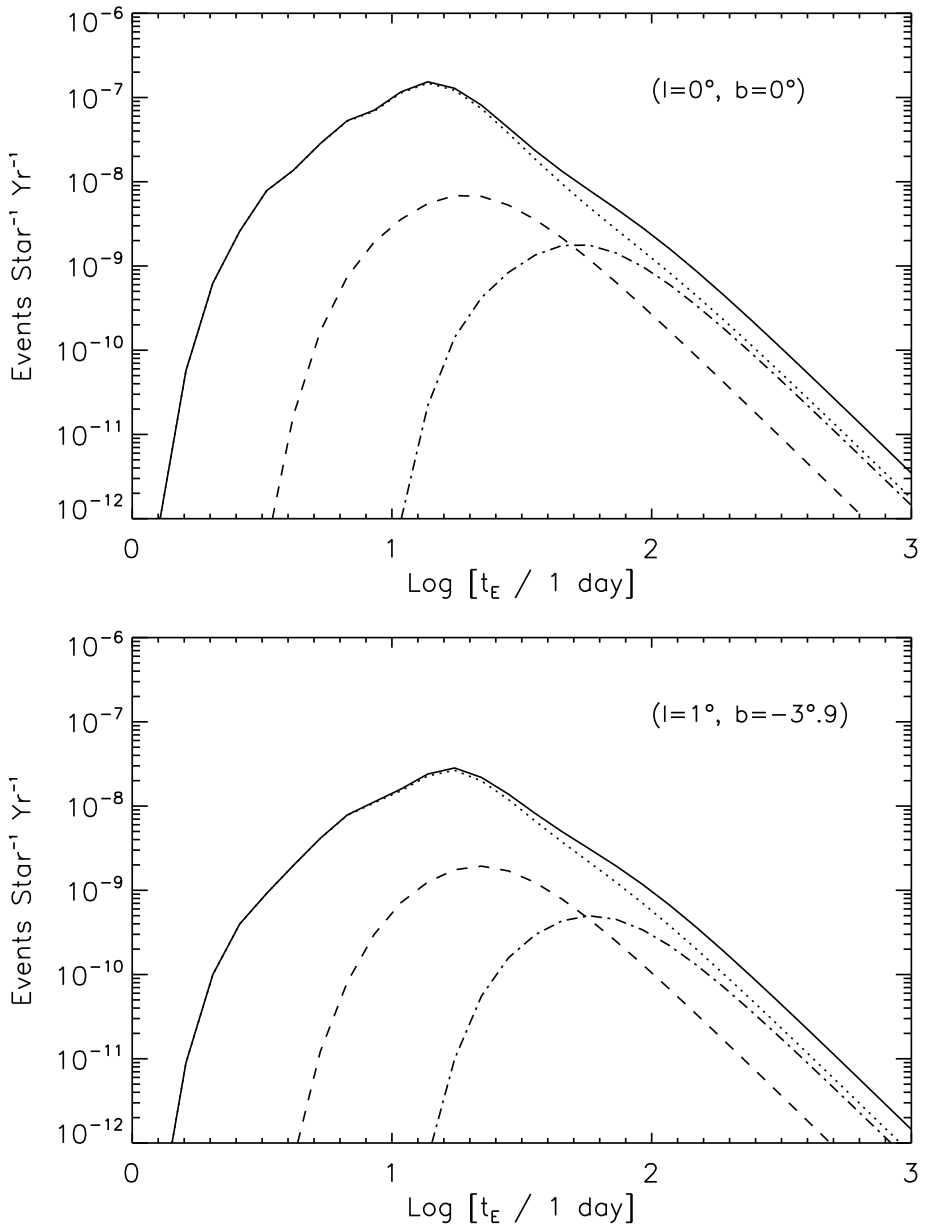

Figure 16: Distribution of time scales for two different l.o.s., $(l, b) = (0°, 0°)$ (top) and $(l, b) = (1°, -3°.9)$ (bottom). Each panel shows the total contribution (solid) and those of normal stars (dotted), neutron stars (dashed) and black holes (dot-dashed), respectively.

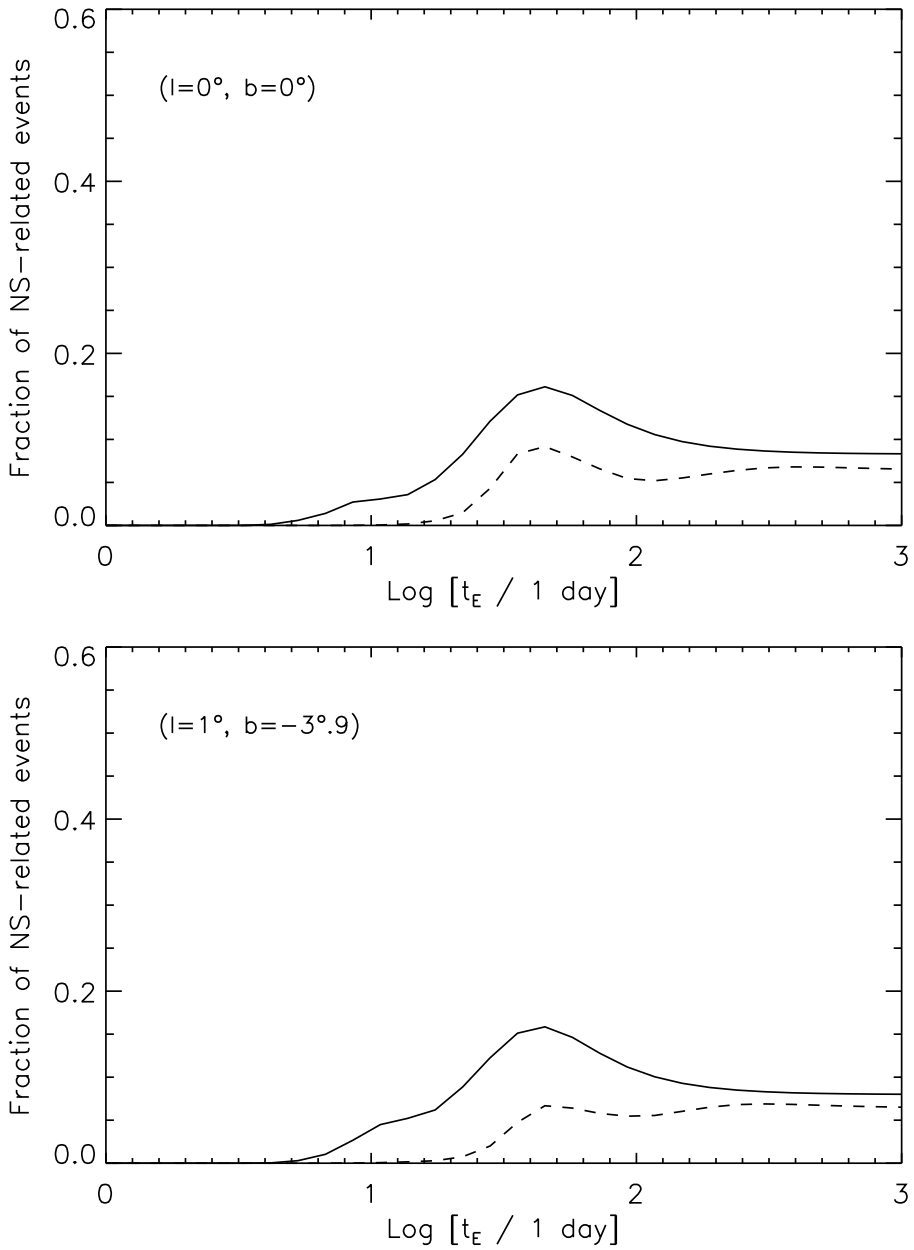

Figure 17: Fractional contribution of neutron stars to the microlensing rate. The l.o.s. are the same of Figure 16. The dashed line represents the expected contribution when kinematic effects are not taken into account.

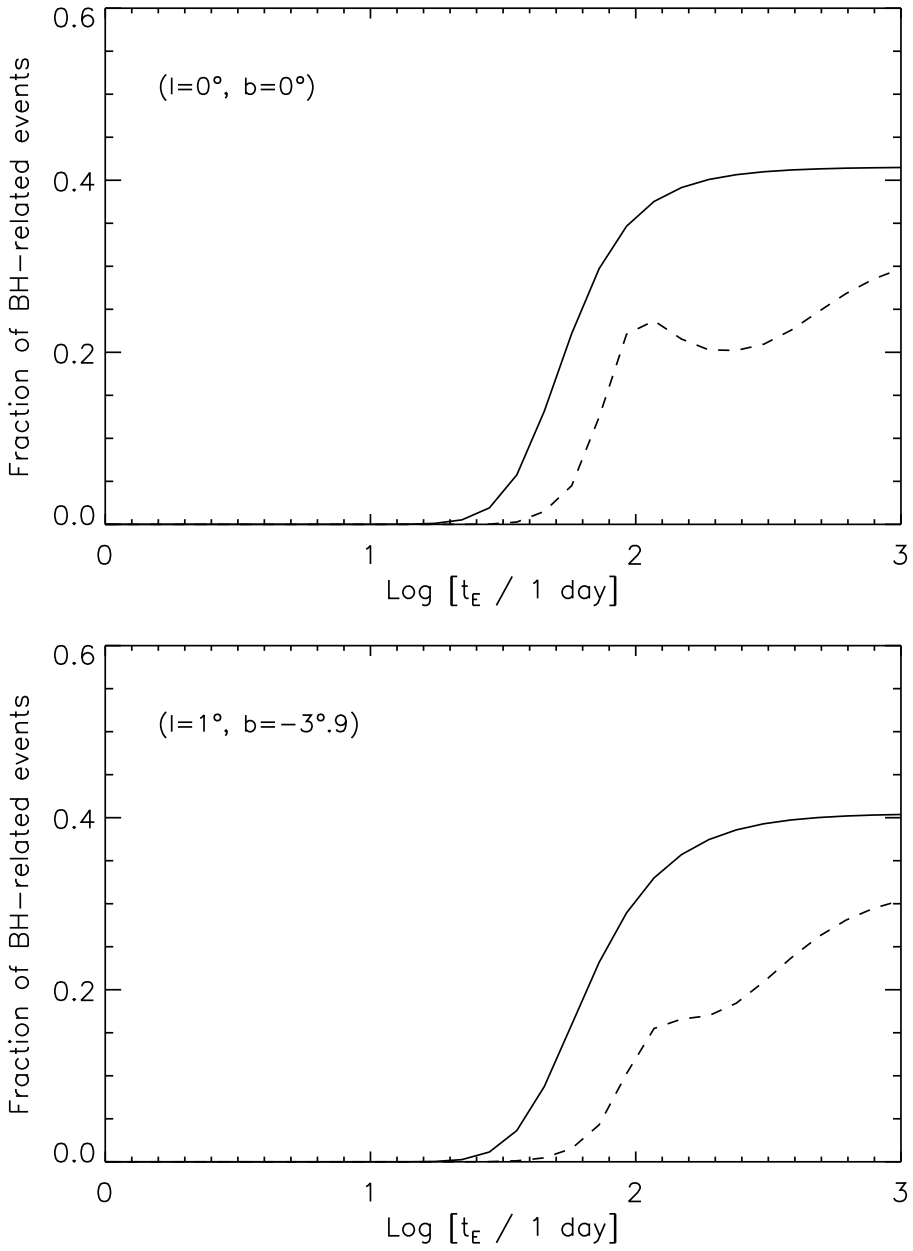

Figure 18: Fractional contribution of black holes to the microlensing rate. Line styles as in Figure 17.

Table 8: Fractional contribution of neutron stars and black holes to the rate of events. The l.o.s. are the same of Table 7.

	l.o.s.	
	$(0°, 0°)$	$(1°, -3°.9)$
f_{NS}		
All	0.05	0.07
$(1 < \log t_E < 2)$	0.06	0.08
$(\log t_E > 2)$	0.10	0.09
f_{BH}		
All	0.01	0.02
$(1 < \log t_E < 2)$	0.01	0.02
$(\log t_E > 2)$	0.38	0.35

3.4.3 Comparison with previous simulations

The results regarding the distribution of neutron stars are now compared to what reported in Chapter 2 and with the results of Ofek. I find that for bulge neutron stars the evaporation from the Galaxy is highly inefficient, that is, almost all bulge-born object are in bound orbits, $f^{(b)}_{bound} \sim 0.98$, because of the large gravitational force towards the inner part of the Milky Way. The fraction of disk-born NSs in bound orbits is slightly lower than what reported in the previous Chapter for the same velocity distribution, $f^{(d)}_{bound} \sim 0.63$ because, as already pointed out, the escape velocity in the new model is also lower. In total, $\sim$ 20 percent of neutron stars evaporated from the Galaxy.

These results are different from those obtained by Ofek (2009), for which $f^{(d)}_{bound} \sim 0.41 - 0.52$ and $f^{(d)}_{bound} \sim 0.13 - 0.16$, for bulge and disk neutron stars , respectively, depending on the selected velocity distribution. The

main reason is the difference in the gravitational potential adopted for the Milky Way. In the model presented here the total mass of the Galaxy is $\sim 10^{12} M_{\odot}$ (e.g. Xue et al., 2008), that is a factor ~ 7 larger than that adopted by Ofek (2009). This translates into a larger fraction of neutron stars is bound orbits.

Bulge-born objects dominate the density of neutron stars in the inner part of the Galaxy, see Figure 19. In particular the density of ONS in the Galactic center bulge can be as high as $\sim 0.12\,\mathrm{pc}^{-3}$, of which ~ 93 percent have been generated in the bulge itself. The density of neutron stars in the solar neighbourhood is $n_0 \sim 3.3 \times 10^{-5}\,\mathrm{pc}^{-3}$, of which only ~ 23 percent comes from the bulge.

In the Galactic center the density of neutron stars reaches $n_{GC} \sim 0.12\,\mathrm{pc}^{-3}$, of which ~ 93 percent have been born in the bulge itself. These results are similar to those of Ofek (2009), who obtained $n_{GC} \sim 0.2 - 0.3\,\mathrm{pc}^{-3}$, with $95-97$ percent of objects being bulge-born. The larger contribution of bulge neutron stars to the density towards the Galactic center can be appreciated for example in Figure 20, where the projected density within 12 kpc from the Sun is $\sim 7.3 \times 10^4\,\mathrm{deg}^{-2}$ against $\sim 6.7 \times 10^3\,\mathrm{deg}^{-2}$ of disk-born neutron stars.

In the case of black holes , because we assumed that they have the same kinematic properties of neutron stars , the density can be easily inferred from that of neutron stars , recalling that the number ratio between black holes and neutron stars should be ~ 0.1, as calculated from the initial mass function.

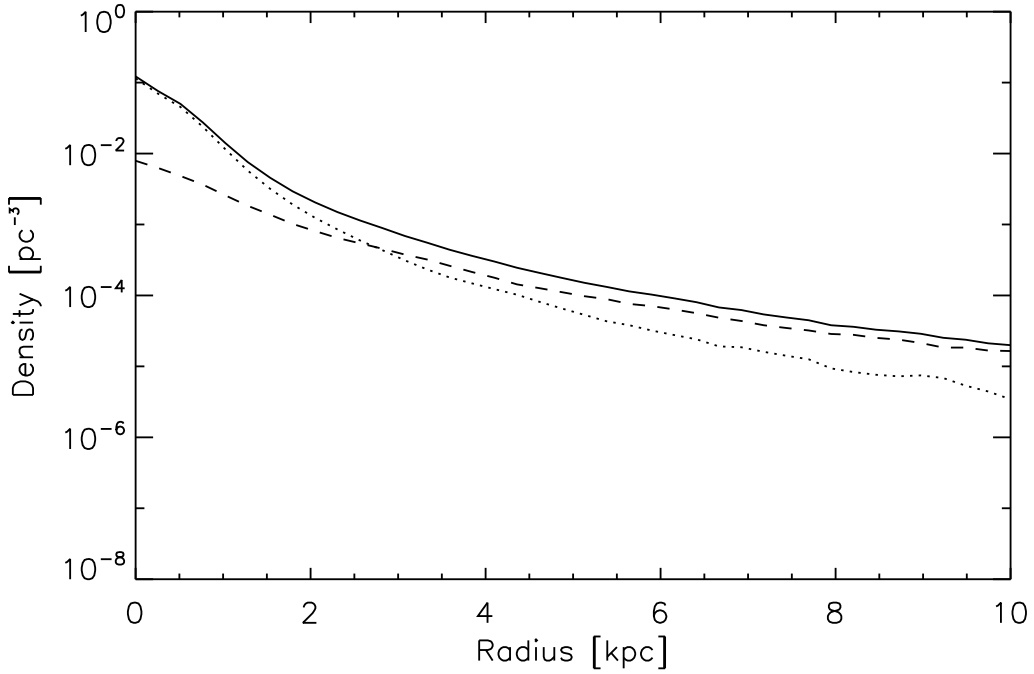

Figure 19: Density profiles of neutron stars in the Galactic plane. Solid, dotted, and dashed lines represent the total, bulge, and disk contributions.

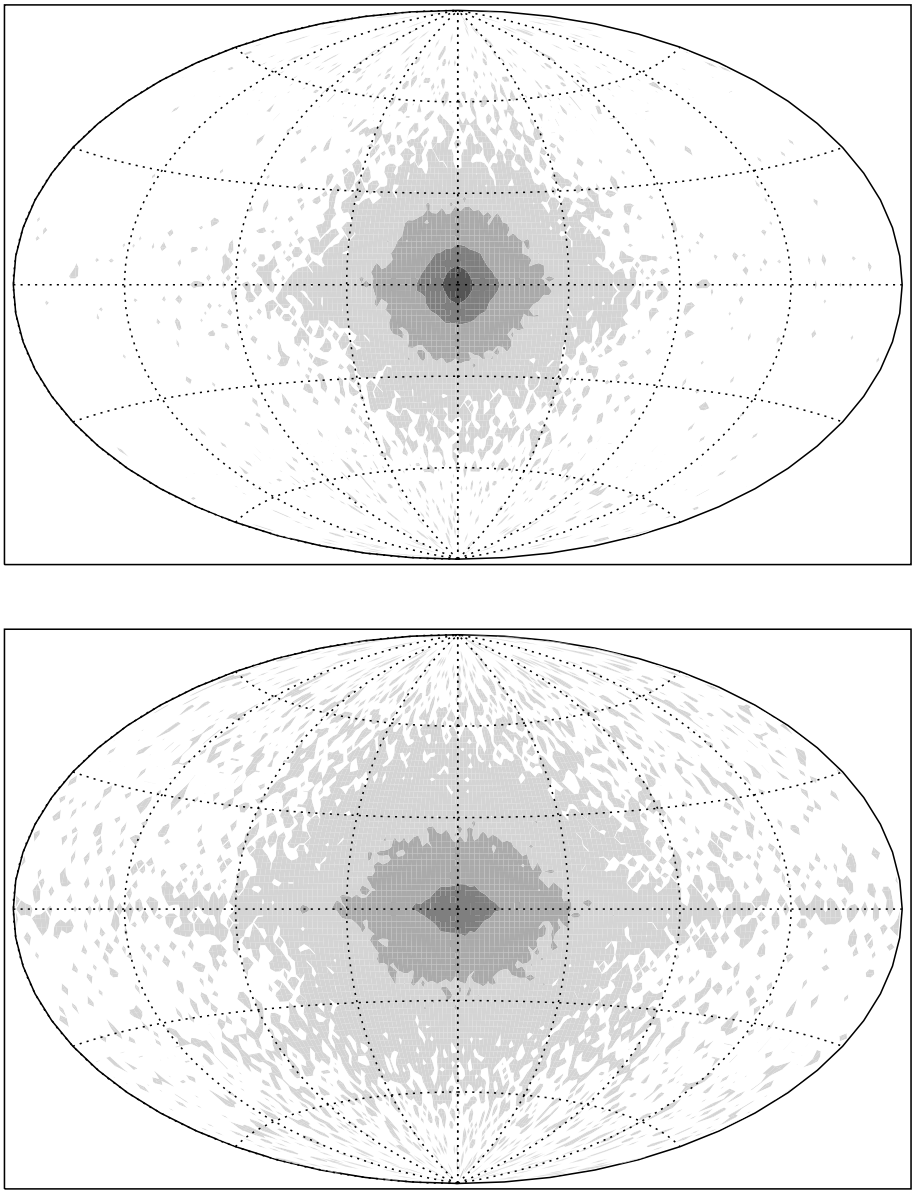

Figure 20: Aitoff projection of the sky density of neutron stars within 12 kpc from the Sun, for bulge-born (upper panel) and disk-born (lower panel) objects. Contour profiles are drawn at $(10, 10^2, 10^3, 10^4)\,\mathrm{deg}^{-2}$, respectively.

3.5 Discussion of the results

The results presented in this Chapter are published in Sartore & Treves (2010). These results underline that the population neutron stars and black holes born in the Galactic bulge may account for a large fraction of the compact remnants in the Milky Way. Even if born with large kick velocities, they are deeply buried in the potential well of the Galaxy and lay in the bulge, or close to it. Thus they give the major contribution to the microlensing rate towards the bulge itself.

So, the net effect of these large velocities, notwithstanding the decrease in the optical depth due to evaporation from the Galaxy of the fastest objects, is an increase of the event rate and a decrease in the typical time-scale of the events. Yet, the relative contribution of neutron stars and black holes is greater for increasing time-scales. Intriguingly, for durations $\gtrsim 100$ days, $\sim 30 - 40$ percent of the events observed could be related to black holes.

Up to date, thousands of events have been observed toward the Galactic bulge by the various surveys (Moniez, 2010). Thus, the results presented here suggest that at least several hundreds of events related to neutron stars and black holes could be already present in the catalogues. These are likely to be hidden among long-duration events. An an excess of long-duration events has indeed been reported by Popowski et al. (2005). These event are likely to be generated by compact massive objects, like compact remnants.

The basic problem is therefore to discuss a procedure to distinguish isolated compact remnants from normal stars that are responsible for the microlensing events. As stated in Chapter 1 the only source of steady luminosity for isolated neutron stars and black holes suggested thus far is accretion from the ISM (e.g. Ostriker et al., 1970; Treves & Colpi, 1991; Blaes & Madau, 1993; Agol & Kamionkowski, 2002). Accretion onto black holes is favoured

with respect to neutron stars , because they are more massive and do not have a magnetic field that can hamper the accretion flow. However, they are far less numerous than neutron stars.

All these considerations should be revisited, because we now consider the remnants in the bulge. The magnetic field of neutron stars and the properties of the ISM are different from what was discussed so far (e.g. Zane et al., 1996). One should first calculate a realistic X-ray luminosity (see e.g. on this line Boldin & Popov, 2010, and references therein), corrected for absorption, and then compare with present and future X-ray missions. The advantage with respect to a blind search of isolated compact remnants is that microlensing events give a precise location of the object.

If these calculations are correct, microlensing could be the only way to probe the velocity distribution of isolated black holes , which has not yet been constrained.

To test these results, in the following Chapter I present a search for candidate black hole lenses among the catalogues of microlensing events.

4 COUNTERPARTS OF CANDIDATE BLACK HOLE LENSES

The large statistics available for microlensing events implies that many events related to black holes should be present in the catalogues. However, the nature of these black hole candidates has to be assessed with independent methods. The mass estimated from microlensing events is in general affected by large uncertainties, given the degeneracy of the time-scale with input parameters like the mass of the lens and the geometry of the source-lens-observer system, that is, on the relative positions and velocities. On the other hand, the detection of X-rays coming from the position of the microlensing event would be a strong hint for the presence of a compact object.

A search for the X-ray counterpart of one of the most promising black hole candidates detected through microlensing has been performed by Nucita et al. (2006, see also Agol & Kamionkowski 2002). However, a 100 ks pointing of XMM-Newton gave no results down to a limiting flux $\sim 10^{-15}\,\mathrm{erg\,s^{-1}}$.

In this Chapter I describe the method and the results of a cross-correlation analysis of long duration microlensing events with the X-ray catalogues of XMM-Newton and Chandra satellites, in order to find isolated black hole candidates with X-ray counterparts. These results have been recently submitted for publication (Sartore & Treves, 2011).

4.1 Method

4.1.1 Catalogues of microlensing events

This search is based on the public data of the OGLE, MACHO and MOA collaborations available on the World Wide Web. Following the results of the previous Chapter, I select only events with time-scale longer than 100 days. The OGLE data[3] were collected with the Early Warning System (EWS, see Udalski, 2003) from 1998 to 2009 and correspond to the OGLE-II and OGLE-III phases of the survey. The number of events detected in the first year (1998) was 41, of which none had a duration longer than 100 days while e.g. in 2008 the number of events detected was 654 with 38 events longer than 100 days. The total number of events from OGLE is 4117, of which 177 fall in our range of interest.

The MACHO survey data[4] were collected from 1993 to 1999 and contain 528 bulge events reported by Thomas et al. (2005) plus the Red Clump Giants events reported by Popowski et al. (2005), totalling 567 events. Of these, 69 are longer than 100 days.

The MOA survey[5] started in 2000, and in 2006 in entered in its second phase. While the number of events detected in 2000 was barely 8, the current detection rate is similar to that of the OGLE-III survey, i.e. $\sim 500 - 600\,\mathrm{events\,yr^{-1}}$. The number of events detected by MOA up to 2010 is 2622, of which 268 show times-scales longer than 100 days.

[3] *http://ogle.astrouw.edu.pl/*

[4] *http://wwwmacho.mcmaster.ca/*

[5] *http://www.phys.canterbury.ac.nz/moa/*

4.1.2 Catalogues of X-ray sources

I search for X-ray counterparts of the selected sample of microlensing events in the version 1.2 of the second XMM-Newton Serendipitous Source Catalogue (2XMM hereafter, Watson et al., 2009) and in the version 1.1 of the *Chandra* Source Catalogue (CSC hereafter, Evans et al., 2010).

The most recent version of the 2XMM catalogue[6] has been released in April 2010. It contains data of 191870 unique sources with a median flux (in the 0.2 - 12 keV band) $\sim 2.5 \times 10^{-14}\,\mathrm{erg\,s^{-1}\,cm^{-2}}$, with 20 percent of the sources having fluxes below $10^{-14}\,\mathrm{erg\,s^{-1}\,cm^{-2}}$.

The CSC catalogue, released in August 2010[7], covers approximately 320 square degrees of the sky at the $10^{-13}\,\mathrm{erg\,s^{-1}\,cm^{-2}}$ flux limit (0.5 - 7.0 keV band). The sky coverage drops to $\sim$ 6 square degrees for a flux limit of $10^{-15}\,\mathrm{erg\,s^{-1}\,cm^{-2}}$. The total number of unique sources contained in the catalogue is 106586.

Most of microlensing events towards the bulge occur in a region of $20^\circ \times 20^\circ$ around the Galactic center, $-10^\circ \leq l \leq 10^\circ$ and $-10^\circ \leq b \leq 10^\circ$. The number of XMM-Newton pointings in this area is $\sim$ 250. This correspond, considering the $30' \times 30'$ field-of-view of the EPIC instruments, to $\sim 50\,\mathrm{deg}^2$. The area covered by Chandra in the same region is expected to be of the same order of magnitude, see Figure 21.

4.1.3 Cross-correlation analysis

Given the large uncertainties affecting the expected observational appearance of old isolated neutron stars and black holes, no particular spectral or variability criteria is applied on possible X-ray counterparts. Nevertheless,

[6] *http://xmmssc-www.star.le.ac.uk/Catalogue/xcat_public_2XMM.html.*

[7] *http://cxc.harvard.edu/csc/.*

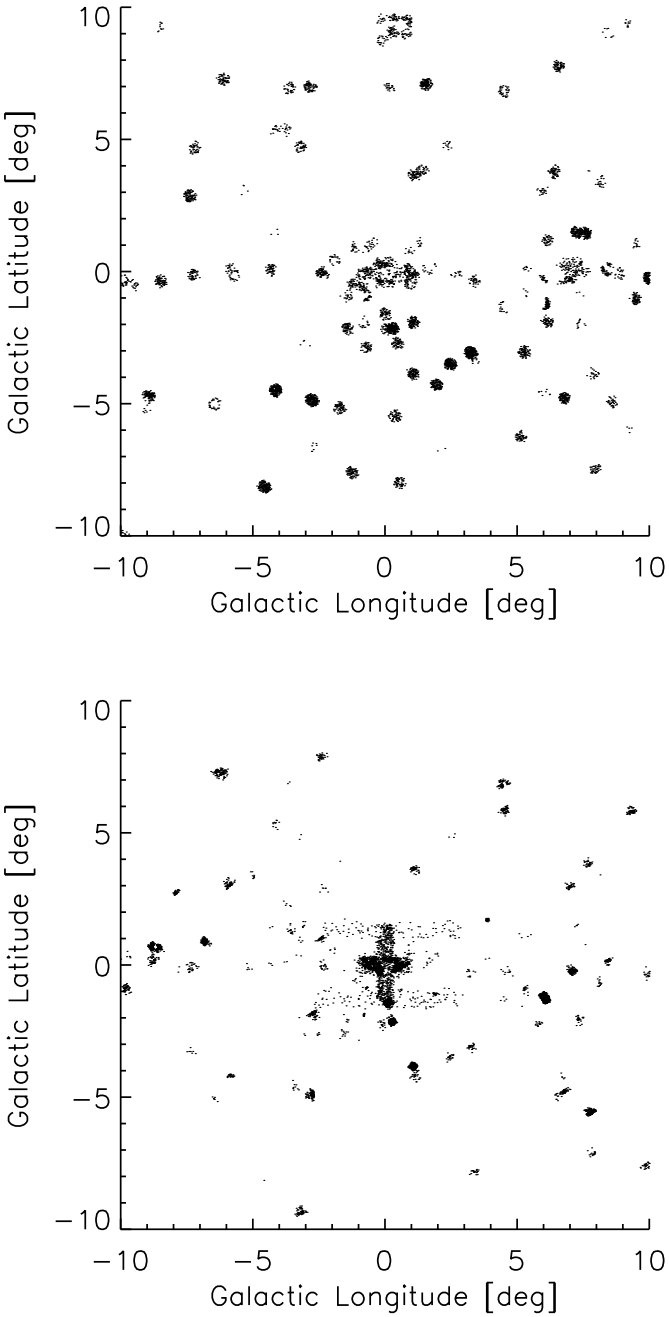

Figure 21: Sky position of the X-ray sources towards the bulge for the 2XMM (top) and CSC (bottom) cataloguess, respectively.

we get rid of spurious sources in the 2XMM catalogue by selecting only those with $SUM\_FLAG = 0$, i.e. those for which none of the warning flags of the EPIC instruments were set. These flags indicate the probability of a detected source to be spurious.

For the CSC catalogue there is no similar flag, but the estimated number of spurious sources is expected to be less than one in every field with 100 kiloseconds of integration. Thus, our matching criterion is based only on the positional coincidence of the long time-scale microlensing events with the X-ray sources of the 2XMM and CSC catalogues.

The cross-correlation routine computes the projected distance between the selected microlensing events and the entries of both the 2XMM and CSC catalogues. A positive match is found when a microlensing event lies with the 3σ error circle of an X-ray source.

Positional errors of single sources are taken from the respective catalogues. The positional error of 2XMM sources ($POSERR$ column) already accounts for systematic errors. The total 1σ uncertainty is calculated as the root mean square of sum of the statistical and systematic errors (Watson et al., 2009)

$$POSERR = \sqrt{RADEC\_ERR^2 + SYSERR^2}\,. \tag{4.1}$$

For CSC sources, to take into account the systematic error (0.16 arc-sec) I use the equation suggested by the CSC team

$$err\_ell\_r_{0,\mathrm{tot}} = 2.4477467 \times \sqrt{0.1669041 \times (err\_ell\_r_{0,\mathrm{cat}})^2 + 0.0256}\,. \tag{4.2}$$

Typically, the statistical error for on-axis CSC sources is ~ 0.2 arc-seconds while for off-axis sources at 14 arc-minutes is ~ 3.5 arc-seconds.

I assume that positional errors of microlensing events are of $\sigma_{ML} \sim 1.5$ arc-seconds for all the microlensing events. Thus, the resulting radius of the error circle is the root mean square of the X-ray source and microlensing event positional uncertainties

$$\sigma = \sqrt{\sigma_{ML}^2 + \sigma_X^2}\,. \tag{4.3}$$

4.2 Results of the cross-correlation

The cross-correlation analysis returned a single positive match in the 2XMM catalogue. The associated lensing event was observed in 2004 by both the OGLE and MOA surveys and is identified as OGLE 2004-BLG-81 and MOA 2004-BLG-3, respectively. The duration of the event reported by the OGLE team is ~ 103.63 days. However, the light curve is poorly fitted by standard lensing models. Wyrzykowski et al. (2006) found that the baseline of the source star, i.e. the magnitude outside the microlensing event (I$\sim$ 17) has a suspected periodicity of ~ 3.9 days, thus pointing to an eclipsing binary. In particular, the shape of the folded light curve points to a contact binary system. This fact would suggest that the event is correlated to a cataclysmic variable (CV) rather than to gravitational microlensing.

To add more confusion, the MOA team reports a baseline $I \sim 8$ (sic!), a duration of ~ 6.73 days and amplification very close to unity, $A \sim 1.002$. However, a visual inspection of the stellar field does not confirm the presence of such a bright star, whose image would have been affected by diffraction.

Thus, I rely on the OGLE data to characterize the event.

The X-ray source associated with the microlensing event, 2XMM J180540.5-273427 (J1805 hereafter), has been serendipitously observed during a pointing of MACHO-96-BLG-5, another black hole candidate detected through microlensing (Bennett et al., 2002; Nucita et al., 2006). The positional uncertainty of the source is ~ 2 arc-seconds and it lies at ~ 0.5 arc-seconds from the position of the microlensing event.

The X-ray properties of the source have been retrieved with the XCat-DB web interface (Motch et al., 2009). The total number of counts is $312.744\,(\pm 0.001)$ (0.2 - 12 keV band) corresponding to a flux of $3.39\,(\pm 0.78)\times 10^{-14}\,\mathrm{erg\,s^{-1}\,cm^{-2}}$.

I report the fluxes on the different EPIC bands and the relative hardness ratios as given in the XCat database (Table 9). Neglecting photoelectric absorption, the luminosity in the 0.2-12 keV band is $\sim 3.8\times 10^{30}\,(D/\mathrm{kpc})^2\,\mathrm{erg\,s^{-1}}$, where D is the distance of the X-ray source in kiloparsec. If J1085 is a massive object responsible for the magnification of a bulge star ($d\sim 8\,\mathrm{kpc}$), then it should be placed at an intermediate distance and its X-ray luminosity should be lower than $\sim 10^{32}\,\mathrm{erg\,s^{-1}}$.

Table 9: Observed properties of the X-ray source 2XMM J180540.5-273427. Data are retrieved on the XCat database. Hardness ratios are calculated as described in Watson et al., with the lower energy band corresponding to the position in the table.

Energy Band [keV]	Flux [$\times 10^{-14}$erg s^{-1} cm^{-2}]	Hardness ratio
0.2-0.5	0.002 ± 0.001	0.982 ± 0.268
0.5-1.0	0.034 ± 0.027	0.738 ± 0.141
1.0-2.0	0.298 ± 0.050	0.132 ± 0.100
2.0-4.5	1.20 ± 0.146	-0.356 ± 0.157
4.5-12	1.73 ± 0.762	

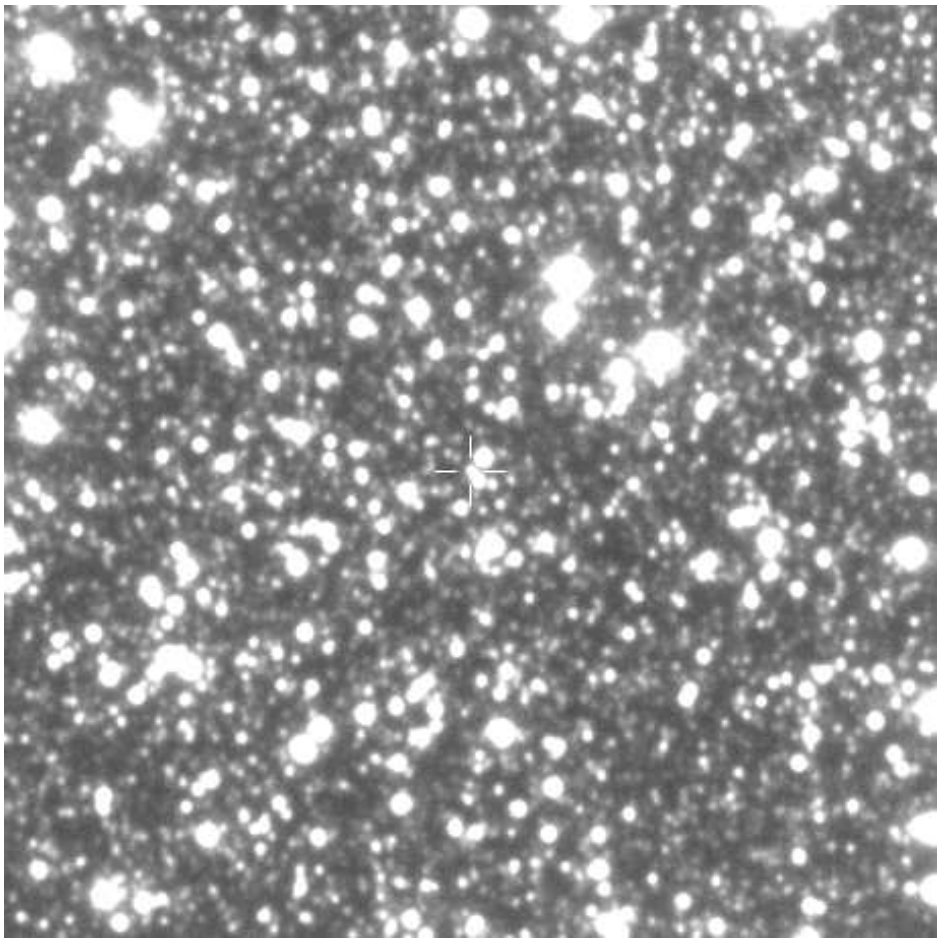

Figure 22: Finding chart of the OGLE 2004-BLG-81 event. Source: OGLE web page.

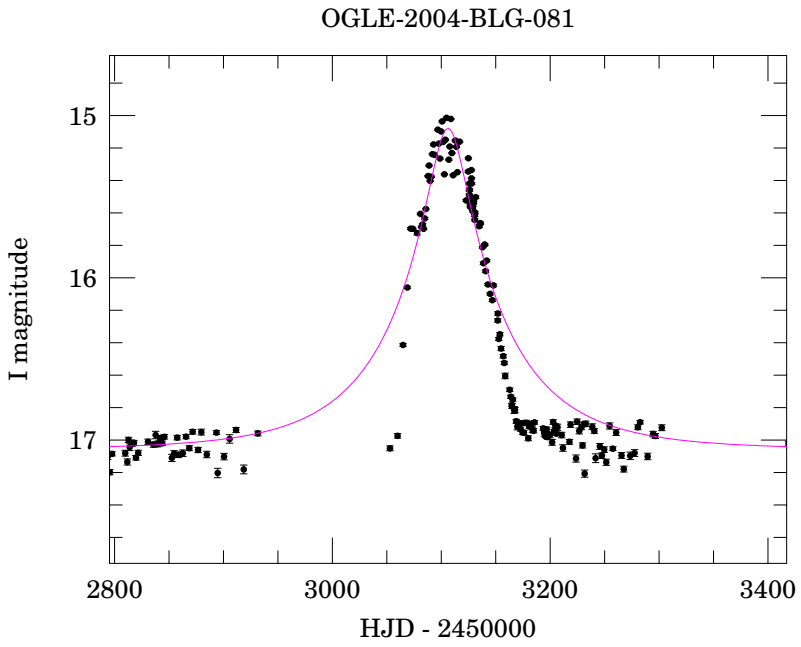

Figure 23: Light curve of the OGLE 2004-BLG-81 event. Solid line represents the best fit of the light curve. Source: OGLE web page.

4.3 The nature of 2XMM J180540.5-273427

The small angular separation ($\sim$ 0.5 arc-seconds) between the position of the microlensing event OGLE 2004-BLG-81 and J1805 is well below the 1σ positional uncertainty of the X-ray source makes the association highly likely. Thus, if J1805 is actually a black hole , it would prove that microlensing surveys can detect isolated compact objects. However, there are a number of uncertainties than need to be addressed to confirm the claim.

First, as Wyrzykowski et al. have pointed out, nature of the microlensing event itself is unclear. The fact that the source star is a contact binary would indicate a cataclysmic variable (CV). However, the duration of the putative outburst is longer than those of classic CVs and the shape of the light curve is different too, thus challenging the CV hypothesis (see e.g. Kuulkers et al., 2003). Then, the symmetry of the light curve still favours microlensing scenario.

Even so, the very nature of the X-ray source J1805 is poorly constrained as well. The small number of photons collected does not allow a good characterization of the spectrum. The hardness ratios are positive at low energies and change sign between 2 and 4.5 keV. This fact would suggest a hard or highly absorbed spectrum. A hard spectrum would rule out a neutron star as accreting object since its temperature is expected to be below $\sim$ 1 keV. Thus, if J1805 is an isolated compact object, it should be a black hole.

5 SUMMARY AND CONCLUSIONS

In this thesis I dealt with the observability of the population of isolated neutron stars and black holes which is expected to be housed in the Milky Way.

To this purpose, I first developed a Monte Carlo-based population synthesis code, in order to simulate the orbits of neutron stars in the gravitational potential of the Galaxy and so to constrain their distribution in phase-space. The results obtained with the code can be summarized as follows.

A non negligible fraction, ~ 30 percent, of the neutron stars born in the Galactic disk have definitely escaped from the Milky Way. Since the mass of the Galaxy has probably increased during the cosmic time, while the star formation rate has likely decreased, neutron stars born in past epochs had greater probability to escape. Thus, the escape fraction reported in Chapters 2 and 3 are lower limits of the true value. Accordingly, the reported values of the surface and spatial densities should be considered as upper limits.

Only less than 20 percent of bound neutron stars is currently found within 200 pc from the Galactic plane, where most of the ISM is found. Typical velocities of these objects are around $150 - 200\,\mathrm{km\,s^{-1}}$ and imply accretion luminosities $\sim 3-4$ orders of magnitude lower than those inferred in previous studies. Neglecting photoelectric absorption, the resulting X-ray fluxes are below the sensitivity limits of the ROSAT survey, even for very close objects.

Neutron stars and black holes born in the bulge account for roughly half of the compact objects in the Milky Way. They are almost all in bound orbits because, being deeply buried in the potential well the the Galaxy, they have a much lower escape probability than disk neutron stars and black holes. From the perspective of an observer at the Earth's position, both populations cluster in the direction of the Galactic bulge, where the more dense Galactic

stellar fields lay. Therefore, neutron stars and black holes can give a non-negligible contribution to the microlensing rate. Indeed, thanks to their large velocities, neutron stars and black holes account for $\sim 5-10$ percent of the total rate of microlensing events towards the bulge. In particular, events related to neutron stars and black holes have on average duration longer than those due to normal stars and can account for ~ 40 percent of the events with duration longer than 100 days.

Thus, microlensing reveals itself as a new, powerful method to find neutron stars and black holes in isolation. Neutron stars and black holes can be detected independently from their intrinsic emission properties and their position in the sky would be known with great accuracy. The only drawback is the uncertainty on the mass of the lens. A confirmation of the nature of neutron star/black holelenses is therefore needed and could come from the observation of counterparts at other wavelengths, for example in the radio or X-ray domains.

A cross-correlation between the catalogues of microlensing events and X-ray sources available returned a single black hole candidate, 2XMM J180540.5-273427, which lies within $\sim$ 0.5 arc-seconds from the microlensing event OGLE 2004-BLG-81, but the nature of both the X-ray source and the microlensing event have few constraints. It should be noted that, even if the association between OGLE 2004-BLG-81 and 2XMM J180540.5-273427 would not be confirmed, the argument that a large fraction of long duration events are related to black holes is still valid. The expected flux from an isolated black hole or neutron star depends on many unknown quantities: the velocity of the collapsed object, the density of the ISM, the photoelectric absorption etc. (see e.g. Chapter 1). Therefore, it is not straightforward to use the absence, or paucity, of correlation between X-ray sources and microlensing

events as a constraint on so many parameters.

In the next years a substantial enlargement of the catalogs of microlensing events and X-ray sources is expected. In particular the eROSITA mission, which should be launched shortly, will make a survey of the entire sky, which in the soft X-ray band (0.5 - 2 keV) will be 30 times more sensitive than ROSAT. At the same time, deep systematic exposures with Chandra and XMM-Newton, of the most promising microlensing events, chosen mainly on the basis of the duration, will also help to set stronger constraints on the flux of accreting isolated compact objects.

A Coefficients of the fits

I give here the best fit parameters for the surface density of the disk (Table 10), the distribution of heights above the Galactic plane (Table 11) and the cumulative velocity distributions in the disk, both in the reference frame at rest with Galactic center sand the frame corotating with the Galactic disk (Table 12).

Table 10: Surface density of the disk.

Model	1A	1B	1C	1D	1E	1A*	1B*	1C*	1D*	1E*
a_0	6.09	6.48	6.51	6.60	6.54	6.24	6.57	6.57	6.66	6.61
a_1 $[\times 10^{-1}]$	-2.54	-2.58	-3.08	-2.79	-1.74	-2.47	-2.41	-2.84	-2.68	-1.83
a_2 $[\times 10^{-2}]$	1.40	1.57	2.37	1.83	0.32	1.05	1.20	1.96	1.79	0.58
a_3 $[\times 10^{-4}]$	-5.69	-8.06	-12.70	-9.20	-2.28	-2.99	-5.25	-10.22	-10.07	0.13
a_4 $[\times 10^{-5}]$	0.90	1.67	2.59	1.82	-0.34	0.22	1.00	2.11	2.25	0.34

Table 11: Distribution of heights.

Model	1A	1B	1C	1D	1E	1A*	1B*	1C*	1D*	1E*
b_0	142.3	87.5	123.1	92.9	112.7	122.7	73.7	115.5	91.5	107.4
b_1	1.12	1.20	1.16	1.22	1.22	1.14	1.25	1.17	1.24	1.24
b_2	-136.3	-83.7	-120.0	-91.0	-111.9	-117.1	-70.6	-112.7	-89.9	-106.8

Table 12: Cumulative velocity distribution in the disk.

Model	1A	1B	1C	1D	1E	1A*	1B*	1C*	1D*	1E*
v_0 $[\mathrm{km\,s^{-1}}]$	214.1	207.4	201.1	200.1	207.2	244.5	241.2	232.5	232.5	238.6
n	3.98	4.56	4.05	4.63	8.09	4.03	4.84	4.16	4.85	8.21
m	3.98	4.56	4.05	4.63	8.09	4.03	4.84	4.16	4.85	8.21
Model	1A	1B	1C	1D	1E	1A*	1B*	1C*	1D*	1E*
v_0' $[\mathrm{km\,s^{-1}}]$	162.4	130.5	169.4	133.5	57.1	178.7	139.7	182.3	141.9	64.4
n'	3.35	3.33	2.77	2.57	1.92	3.34	3.35	2.70	2.50	1.94
m'	2.35	3.33	2.76	2.57	1.92	3.34	3.35	2.70	2.50	1.94

List of publications

Refereed papers

"VLT/MAD observations of the isolated neutron stars RX J0420.0-5022 and RX J1856.5-3754". R. P. Mignani, Falomo, R., A. Moretti, A. Treves, R. Turolla, **N. Sartore**, S. Zane, et al., 2008, A&A, 488, 267 (arXiv:0806.4136).

"Galactic neutron stars. I. Space and velocity distributions in the disk and in the halo of the Milky Way". **N. Sartore**, E. Ripamonti, A. Treves & R. Turolla, 2010, A&A, 510, A23 (arXiv:0908.3182).

"Probing isolated compact remnants with microlensing". **N. Sartore** & A. Treves, 2010, A&A, 523, A33 (arXiv:1009.0005).

Submitted/under referee papers

"Matching microlensing events with X-ray sources". **N. Sartore** & A. Treves, 2011, A&A, submitted

Refereed proceedings

"Space and velocity distributions of neutron stars in the Milky Way". **N. Sartore**, E. Ripamonti, A. Treves & R. Turolla, 2011, AdSpR, 47, 1294-1297.

Papers in preparation

"Long term monitoring RX J1856.5-3754. Analysis of EPIC-pn data". **N. Sartore**, A. Tiengo, S. Mereghetti et al.

"Fast halo millisecond pulsars ejected by intermediate mass blach holes in globular clusters". A. Sesana, B. Devecchi, **N. Sartore**, A. Possenti et al.

"The search for the birthplace of the isolated neutron star RX J1856.5-3754". R. P. Mignani, D. Vande Putte, M. Cropper, C. Motch, L. J. Pellizza, **N. Sartore** et al.

Acknowledgments

First, I would like to thank Prof. Roberto Turolla for the stimulating discussions and the help during all phases of my PhD project. I also thank Dr. Emanuele Ripamonti for helping me to debug the first version of the PSYCO code. A special thanks goes to Dr. Ruben Salvaterra and Luca Paredi for their support in many of the issues I found during the PhD work.

I would also like to express my gratitude to all the people met during my stay at Como, for their friendship and kindness, in particular those from the "Ufficio Astrofisici": Massimo Cavadini, Maura Pilia, Emanuele Paolo Farina, Dr. Massimo Dotti, Dr. Roberto Decarli, Dr. Marco Ramilli, Luca Paredi, Dr. Ruben Salavaterra, Dr. Maria Angela Campisi, Dr. Bernadetta Devecchi, Dr. Alberto Sesana, Carmen Montuori, Giorgia Pollina, Martina Barattini, Matteo Sala, Prof. Francesco Haardt and all the others that are not listed but not forgotten.

Last but not least I would like to thank Valeria for her unconditional support during these long years, in either the nice and bad moments.

To all of you, thanks!

References

Agol, E., & Kamionkowski, M. 2002, MNRAS, 334, 553

Alcock, C., et al. 1993, Nature, 365, 621

Alcock, C., et al. 1997, ApJ, 479, 119

Alpar, M. A., Cheng, A. F., Ruderman, M. A., & Shaham, J. 1982, Nature, 300, 728

Arnett, W. D., Schramm, D. N., & Truran, J. W. 1989, ApJL, 339, L25

Arzoumanian, Z., Chernoff, D. F., & Cordes, J. M. 2002, ApJ, 568, 289

Aubourg, E., et al. 1993, The Messenger, 72, 20

Bennett, D. P., et al. 2002, ApJ, 579, 639

Beskin, G. M., & Karpov, S. V. 2005, A&A, 440, 223

Blaes, O., & Madau, P. 1993, ApJ, 403, 690

Boldin, P. A., & Popov, S. B. 2010, MNRAS, 407, 1090

Bondi, H., & Hoyle, F. 1944, MNRAS, 104, 273

Bondi, H. 1952, MNRAS, 112, 195

Bower, G. C., Saul, D., Bloom, J. S., Bolatto, A., Filippenko, A. V., Foley, R. J., & Perley, D. 2007, ApJ, 666, 346

Brisken, W. F., Fruchter, A. S., Goss, W. M., Herrnstein, R. M., & Thorsett, S. E. 2003, AJ, 126, 3090

Bronfman, L., Casassus, S., May, J., & Nyman, L.-Å. 2000, A&A, 358, 521

Calchi Novati, S., de Luca, F., Jetzer, P., Mancini, L., & Scarpetta, G. 2008, A&A, 480, 723

Campana, S., & Pardi, M. C. 1993, A&A, 277, 477

Case, G. L., & Bhattacharya, D. 1998, ApJ, 504, 761

Chatterjee, S., et al. 2005, ApJL, 630, L61

Chiappini, C., Matteucci, F., & Romano, D. 2001, ApJ, 554, 1044

Colpi, M., Turolla, R., Zane, S., & Treves, A. 1998, ApJ, 501, 252

Contopoulos, G., Gottesman, S. T., Hunter, J. H., Jr., & England, M. N. 1989, ApJ, 343, 608

Cordes, J. M., & Lazio, T. J. W. 2002, arXiv:astro-ph/0207156

de Rujula, A., Jetzer, P., & Masso, E. 1991, MNRAS, 250, 348

Dewey, R. J., & Cordes, J. M. 1987, ApJ, 321, 780

Diehl, R., et al. 2006, Nature, 439, 45

Einstein, A. 1936, Science, 84, 506

Evans, I. N., et al. 2010, ApJS, 189, 37

Faucher-Giguère, C.-A., & Kaspi, V. M. 2006, ApJ, 643, 332

Freudenreich, H. T. 1998, ApJ, 492, 495

Gould, A. 2000, ApJ, 535, 928

Griest, K. 1991, ApJ, 366, 412

Gualandris, A., Colpi, M., Portegies Zwart, S., & Possenti, A. 2005, ApJ, 618, 845

Gvaramadze, V. V., Gualandris, A., & Portegies Zwart, S. 2008, MNRAS, 385, 929

Jetzer, P., Mancini, L., & Scarpetta, G. 2002, A&A, 393, 129

Hamadache, C., et al. 2006, A&A, 454, 185

Hartmann, D., Woosley, S. E., & Epstein, R. I. 1990, ApJ, 348, 625

Heger, A., Fryer, C. L., Woosley, S. E., Langer, N., & Hartmann, D. H. 2003, ApJ, 591, 288

Hernquist, L. 1990, ApJ, 356, 359

Hobbs, G., Lorimer, D. R., Lyne, A. G., & Kramer, M. 2005, MNRAS, 360, 974

Hui, C. Y., & Becker, W. 2006, A&A, 457, L33

Iben, I., Jr., & Tutukov, A. V. 1996, ApJ, 456, 738

Illarionov, A. F., & Sunyaev, R. A. 1975, A&A, 39, 185

Keane, E. F., & Kramer, M. 2008, MNRAS, 391, 2009

Kiel, P. D., & Hurley, J. R. 2009, MNRAS, 395, 2326

Kiraga, M., & Paczynski, B. 1994, ApJL, 430, L101

Kroupa, P. 2001, MNRAS, 322, 231

Kuulkers, E., Norton, A., Schwope, A., & Warner, B. 2003, arXiv:astro-ph/0302351

Lorimer, D. R., Bailes, M., & Harrison, P. A. 1997, MNRAS, 289, 592

Lorimer, D. R. 2008, Living Reviews in Relativity, 11, 8

Maíz-Apellániz, J. 2001, AJ, 121, 2737

Mapelli, M., Ferrara, A., & Rea, N. 2006, MNRAS, 368, 1340

Mereghetti, S. 2008, A&A Rev., 15, 225

Mirabel, I. F., Dhawan, V., Mignani, R. P., Rodrigues, I., & Guglielmetti, F. 2001, Nature, 413, 139

Mirabel, I. F., Mignani, R., Rodrigues, I., Combi, J. A., Rodríguez, L. F., & Guglielmetti, F. 2002, A&A, 395, 595

Miyamoto, M., & Nagai, R. 1975, AJ, 27, 533

Moniez, M. 2010, General Relativity and Gravitation, 42, 2047

Motch, C., Pires, A. M., Haberl, F., Schwope, A., & Zavlin, V. E. 2009, A&A, 497, 423

Muno, M. P., et al. 2006, ApJL, 636, L41

Muraki, Y., et al. 1999, Progress of Theoretical Physics Supplement, 133, 233

Navarro, J. F., Frenk, C. S., & White, S. D. M. 1996, ApJ, 462, 563

Neuhäuser, R., & Trümper, J. E. 1999, A&A, 343, 151

Nucita, A. A., De Paolis, F., Ingrosso, G., Elia, D., de Plaa, J., & Kaastra, J. S. 2006, ApJ, 651, 1092

Ofek, E. O. 2009, PASP, 121, 814

Ofek, E. O., Breslauer, B., Gal-Yam, A., Frail, D., Kasliwal, M. M., Kulkarni, S. R., & Waxman, E. 2010, ApJ, 711, 517

Ostriker, J. P., Rees, M. J., & Silk, J., 1970, Astrophys. Letters, 6, 179

Paczynski, B. 1986, ApJ, 304, 1

Paczynski, B. 1990, ApJ, 348, 485

Paczynski, B. 1991, ApJL, 371, L63

Perna, R., Narayan, R., Rybicki, G., Stella, L., & Treves, A. 2003, ApJ, 594, 936

Picaud, S., & Robin, A. C. 2004, A&A, 428, 891

Popov, S. B., Colpi, M., Treves, A., Turolla, R., Lipunov, V. M., & Prokhorov, M. E. 2000, ApJ, 530, 896

Popov, S. B., Turolla, R., Prokhorov, M. E., Colpi, M., & Treves, A. 2005, Ap&SS, 299, 117

Popowski, P., et al. 2005, ApJ, 631, 879

Posselt, B., Popov, S. B., Haberl, F., Trümper, J., Turolla, R., & Neuhäuser, R. 2008, A&A, 482, 617

Press, W. H., Teukolsky, S. A., Vetterling, W. T., & Flannery, B. P. 1992, Cambridge: University Press, |c1992, 2nd ed.,

Reid, M. J., et al. 2009, ApJ, 700, 137

Rich, R. M., Reitzel, D. B., Howard, C. D., & Zhao, H. 2007, ApJL, 658, L29

Robin, A. C., Reylé, C., Derrière, S., & Picaud, S. 2003, A&A, 409, 523

Salpeter, E. E. 1955, ApJ, 121, 161

Sartore, N., Ripamonti, E., Treves, A., & Turolla, R. 2010, A&A, 510, A23

Sartore, N., & Treves, A. 2010, A&A, 523, A33

Sartore, N., & Treves, A. 2011, A&A, submitted

Smith, M. C., et al. 2007, MNRAS, 379, 755

Stanek, K. Z., Udalski, A., Szymanski, M., Kaluzny, J., Kubiak, M., Mateo, M., & Krzeminski, W. 1997, ApJ, 477, 163

Sumi, T., et al. 2006, ApJ, 636, 240

Sun, X. H., & Han, J. L. 2004, MNRAS, 350, 232

Taylor, J. H., & Cordes, J. M. 1993, ApJ, 411, 674

Thomas, C. L., et al. 2005, ApJ, 631, 906

Toropina, O. D., Romanova, M. M., Toropin, Y. M., & Lovelace, R. V. E. 2003, ApJ, 593, 472

Treves, A., & Colpi, M. 1991, A&A, 241, 107

Treves, A., Turolla, R., Zane, S., & Colpi, M. 2000, PASP, 112, 297

Turolla, R. 2009, Astrophysics and Space Science Library, 357, 141

Udalski, A., Szymanski, M., Kaluzny, J., Kubiak, M., & Mateo, M. 1992, Acta Astron., 42, 253

Udalski, A., et al. 1994, Acta Astron., 44, 165

Udalski, A. 2003, Acta Astron., 53, 291

Vietri, M., & Ostriker, J. P. 1983, ApJ, 267, 488

Xue, X. X., et al. 2008, ApJ, 684, 1143

Yusifov, I., & Küçük, I. 2004, A&A, 422, 545

Walter, F. M., & Matthews, L. D. 1997, Nature, 389, 358

Watson, M. G., et al. 2009, A&A, 493, 339

White, N. E., & van Paradijs, J. 1996, ApJL, 473, L25

Wood, A., & Mao, S. 2005, MNRAS, 362, 945

Wyrzykowski, L., Udalski, A., Mao, S., Kubiak, M., Szymanski, M. K., Pietrzynski, G., Soszynski, I., & Szewczyk, O. 2006, Acta Astron., 56, 145

Zane, S., Turolla, R., Zampieri, L., Colpi, M., & Treves, A. 1995, ApJ, 451, 739

Zane, S., Turolla, R., & Treves, A. 1996, ApJ, 471, 248